https://doi.org/10.5194/egusphere-2025-6528
Preprint. Discussion started: 16 February 2026


# Evaluating national, state, and urban Indian methane emissions using satellites

Srijana Lama[1], Joannes D. Maasakkers[1], Xin Zhang[1], Marianne Girard[2], Swarna Dutt[3], Suyash Nandgaonkar[3], Daniel J. Varon[4], Melissa P. Sulprizio[5], Lucas A. Estrada[5], Nicholas Balasus[5], Robert J. Parker[6,7], Yukio Terao[8], and Ilse Aben[1,9]

[1]SRON Space Research Organization Netherlands, 2333 CA Leiden, The Netherlands
[2]GHGSat Inc., Montréal, Canada
[3]Energy Policy Institute at the University of Chicago (EPIC India), New Delhi, India
[4]Department of Aeronautics and Astronautics, Institute for Data, Systems, and Society, Massachusetts Institute of Technology, Cambridge, MA 02139
[5]School of Engineering and Applied Sciences, Harvard University, Cambridge, MA 02138
[6]National Center for Earth Observations, University of Leicester, Leicester, UK
[7]Earth Observation Science, School of Physics and Astronomy, University of Leicester, Leicester, UK
[8]National Institute for Environmental Studies, Japan
[9]Department of Earth Sciences, Vrije Universiteit Amsterdam, Amsterdam, the Netherlands

*Correspondence to*: Srijana Lama (s.lama@sron.nl, sreejanalama@gmail.com)

**Abstract**

Understanding the spatial distribution and magnitude of methane emissions is critical for developing effective mitigation strategies, particularly in rapidly growing economies like India, the world's most populous country and a top global methane emitter with diverse emission sources. We quantify India's 2021 methane emissions at up to 0.25°×0.3125° resolution using TROPOspheric Monitoring Instrument (TROPOMI) observations in a Bayesian inversion with the Integrated Methane Inversion framework (IMI). Prior emissions come from state-of-the-art global gridded bottom-up inventories and incorporate GHGSat-based estimates for eighteen landfills. The high-resolution inversion and incorporation of GHGSat data enable us to evaluate and interpret results at multiple policy-relevant scales. The national posterior emission estimate is 34.4 (32.0 – 40.4) Tg/yr, of which 31.5 (29.6 – 36.7) Tg $yr^{-1}$ is anthropogenic, consistent with bottom-up prior emissions but 68% higher than India's UNFCCC inventory. National landfill and oil & gas emissions are 30% higher, while coal emissions are 57% lower than prior estimates. State-level analysis highlights seven states with higher emissions, with notably higher oil and gas emissions in Assam and Gujarat, and lower coal mining emissions in Rajasthan and Odisha. Urban-scale posterior estimates for fourteen cities reveal significant differences from the prior in ten cities. Posterior wastewater emissions are higher in nine cities, with the largest increases in Kolkata and Delhi, consistent 60–90% of their populations lacking access to wastewater treatment facilities. GHGSat observations reveal landfills contribute 10-38% of emissions in eleven cities, emphasizing the critical role of solid waste management. These results illustrate how satellite-based analyses can inform methane mitigation.

https://doi.org/10.5194/egusphere-2025-6528
Preprint. Discussion started: 16 February 2026


## 1. Introduction

Methane is the second most important anthropogenic greenhouse gas in terms of radiative forcing, with a global warming potential 27-30 times greater than that of $CO_2$ over a 100-year time scale (Forster et al., 2021). Globally, its atmospheric concentration had increased by more than 160 % in 2021 compared to preindustrial levels, primarily driven by anthropogenic emissions (Skeie et al., 2023). After a period of stability in the early 2000s, methane concentrations have been increasing at an average rate of 7.1 ppb $a^{-1}$ since 2007, with peak growth rates exceeding 10 ppb $a^{-1}$ from 2014 to 2015 and 2020 to 2022 (Lan et al., 2025). Reducing methane emissions has become a key focus of climate agreements like the Paris Agreement and the rapid atmospheric growth highlights the urgency of emission mitigation. The Global Methane Pledge, launched at the 2021 United Nations Climate Change Conference (COP26), has by January 2025 been signed by 159 countries committing to reduce methane emissions by 30 % between 2020 and 2030 (Climate and Clean air Coalition, 2025). South Asia is one of the largest methane emission hotspots globally (Stavert et al., 2022), estimated to emit 52 (43–60) Tg $yr^{-1}$ in total in 2010-2019 and contributing approximately 12 % of global anthropogenic methane emissions (Saunois et al., 2025). The region comprises diverse methane emission sources, including agriculture, waste, wetlands, and energy production, making it a complex area to study (Belikov et al., 2024). Here, we use satellite observations to estimate the methane emissions from India, the third-largest methane emitter globally with reported methane emissions of 18.8 Tg $yr^{-1}$ for 2020 (MoEFCC, 2024).

Recent advancements in satellite remote sensing technology have helped to accurately estimate global methane concentrations with higher spatial and temporal resolution. Earlier satellites such as the Scanning Imaging Absorption SpectroMeter for Atmospheric ChartographY (SCIAMACHY; 2003 -2012) and Greenhouse Gases Observing Satellite (GOSAT) are limited by coarse spatial resolution or sparse coverage (Bovensmann et al., 1999; Butz et al., 2011). The TROPOspheric Monitoring Instrument (TROPOMI), launched in October 2017, provides daily global methane total column observations with a spatial resolution of 5.5 km x 7 km at the nadir (7 km x 7 km before August 2019), greatly enhancing coverage (Hu et al., 2018; Lorente et al., 2021). Inverse modeling methods combine (satellite) observations with atmospheric transport models to link the observations with emissions (Jacob and Brasseur, 2017). These analyses use ‘bottom-up’ activity-based emission estimates as starting point, enabling the evaluation of those estimates and emission mitigation policies. Furthermore, high-resolution (~25m) satellite data, such as from GHGSat and hyperspectral imagers such as Environmental Mapping and Analysis Program (EnMAP) and Earth Surface Mineral Dust Source Investigation (EMIT), have enabled the estimation of emissions from individual facilities such as landfills (Maasakkers et al., 2022; Thorpe et al., 2023; Zhang et al., 2025; Dogniaux et al., 2025). These independent ‘top-down’ analyses can be particularly valuable for highlighting regions, sectors, and facilities where further investigation and stakeholder engagement are warranted.

India is the world’s most populous country, with approximately 1.47 billion residents in 2025 (United Nations Population Fund, 2026). The Indian government’s 2024 Biennial Update Report to the United Nations Framework Convention on Climate Change (UNFCCC) estimates anthropogenic methane emissions for 2020 at 18.8 Tg/yr. An alternate anthropogenic emission

https://doi.org/10.5194/egusphere-2025-6528
Preprint. Discussion started: 16 February 2026


estimate of 22.0 Tg $yr^{-1}$ for 2018 that includes state-level estimates is available from GHG platform India (Solanki et al., 2022; retrieved from https://www.ghgplatform-india.org/afolu-sector-analytics/ on February 10, 2025). The GHG Platform India highlights livestock, waste, rice cultivation, coal, and oil and gas as the major anthropogenic methane sources in India, underscoring the diversity of sources. These inventories use bottom-up methods that rely on activity data and laboratory-based emission factors that can come with significant uncertainties, which can be exacerbated due to lack of (homogenous) reporting capacity, inconsistent methodologies, and high levels of informality in the economy (Gao et al., 2021; MoEFCC 2024). Furthermore, India lacks a comprehensive ground-based measurement network to provide a detailed validation of national estimates (Belikov et al., 2024; Chandra et al., 2017; Guha et al., 2018). India has not signed the Global Methane Pledge, citing concerns that its highest-emitting sectors, agriculture and livestock are 'survival emissions' from small and marginal farmers whose incomes cannot be jeopardized (MoEFCC, 2021). While India's Updated Nationally Determined Contribution (2022) has an economy-wide emissions intensity reduction target to 45% by 2030, this commitment is 'gas-agnostic' and does not specify sectoral methane mitigation strategies (Government of India, 2022).

Several studies have used satellite and surface observations to estimate Indian methane emissions. Ganesan et al. (2017) estimated India's anthropogenic methane emissions at 22.0 (19.6 - 24.3) Tg $yr^{-1}$ for 2010–2015 using GOSAT, surface, and aircraft data in an inverse analysis. Similarly, Janardanan et al. (2020) reported anthropogenic methane emissions of 24.2 Tg $yr^{-1}$ for 2010 to 2017 using an inversion method with GOSAT and aircraft data. Zhang et al. (2021) estimated much higher anthropogenic emissions of 33 Tg $yr^{-1}$ for 2010 to 2018 based on an inversion of GOSAT data. Raju et al. (2022) focused on peninsular India (latitudes below 21.5 °N), estimating methane emissions at 10.6 Tg $yr^{-1}$ for 2017 to 2018 using ground-based data and inverse modelling. Belikov et al. (2024) estimated India's total methane emissions at 45.3 Tg $yr^{-1}$ for 2002 to 2020 using background methane measurements from the ObsPack GLOBALVIEW (Schultd et al., 2021), along with surface flask measurements in Nainital (India) and Comilla (Bangladesh). This estimate is notably higher than previous studies, though it may be influenced by the limited ground-based data. Recently, Subramanian et al. (2025) estimated methane emissions over South Asia for 2020 at 0.5° x 0.5° spatial resolution using a Bayesian inversion framework that combines TROPOMI observations from the Weighting Function Modified Differential Optical Absorption Spectroscopy (WFM-DOAS) product (Schneising et al., 2023) with the Lagrangian transport model FLEXPART, yielding an estimate of India's methane emissions of 35.6 ± 0.5 Tg $yr^{-1}$. Finally, Mathew et al. (2025) quantified India's anthropogenic methane emissions for 2018–2019 at 24.3 (23.3–25.2) Tg $yr^{-1}$ using WFM-DOAS TROPOMI data and the Weather Research and Forecasting model coupled with Chemistry and Greenhouse Gas module (WRF-GHG) to optimize emissions per state. Hence, multiple studies have mainly focused on evaluating emissions at the national (to state) scale and found higher anthropogenic emissions than included in bottom-up emission inventories. For example, India's UNFCCC-reported emissions for 2020 are 19-75% lower than the estimates by Janardanan et al. (2020), Zhang et al. (2021), and Mathew et al. (2025). Similarly, the GHG platform India estimate is 10 - 50% lower than the same studies.

https://doi.org/10.5194/egusphere-2025-6528
Preprint. Discussion started: 16 February 2026


Urban methane emissions in India in particular come with large uncertainty and are linked with significant environmental concerns and public health risks, primarily due to poor waste management practices and the high organic content of municipal solid waste (Siddiqui et al., 2024). India's waste sector constituted approximately 14% of total methane emissions as of 2020, establishing it as a critical non-agriculture pathway for methane reduction (MoEFCC, 2024). Maasakkers et al. (2022) used TROPOMI observations with the Weather Research and Forecasting (WRF) model to estimate urban methane emissions in four cities, including two in India. They found that urban emissions were underestimated in the EDGAR bottom-up inventory and used GHGSat observations to estimate that landfills in Mumbai and Delhi contributed 26% and 6% to their respective urban methane emissions. Foy et al. (2023) estimated methane emissions of seven Indian cities using TROPOMI data combined with a two-dimensional Gaussian model, positing that untreated wastewater could be the largest contributor to urban methane emission. Using 2021-2022 GHGSat observations, Dogniaux et al. (2025) reported emissions from 151 landfills across 130 urban areas, including 18 Indian landfills. They compared the GHGSat estimated emissions with the Climate Tracking Real-time Atmospheric Carbon Emissions (Climate TRACE) dataset (Climate TRACE, 2024) that provides facility-level methane emissions, finding poor correlation. Similarly, Zhang et al. (2025) also found poor agreement between landfill emissions estimated using hyperspectral satellite observations and Climate TRACE.

In this study, we utilize 2021 data from the blended TROPOMI+GOSAT data product (Balasus et al., 2023) in a Bayesian inversion to infer annual methane emissions over India up to resolution of 0.25° x 0.3125°, complemented by GHGSat landfill data available for the same year. We compare national total and sectoral emissions with UNFCCC and bottom-up estimates. Furthermore, we also compare our results with state-level emissions provided by the GHG platform India and analyze methane emissions over 14 urban areas with a focus on waste emissions by incorporating site-level estimates from GHGSat for landfills.

## 2. Data and Method

We perform an inversion of 2021 data from the TROPOMI+GOSAT blended product (Balasus et al., 2023) using the Integrated Methane Inversion (IMI) framework (Varon et al., 2022; Estrada et al., 2025). The satellite observations are used in an analytical Bayesian inversion with log-normal error characterization to optimize 2021 methane emissions at a spatial resolution of up to 0.25° x 0.3125°. We use the GEOS-Chem chemical transport model as the forward model for the inversion and evaluate the results with additional satellite and surface observations. Results from the inversion are aggregated at multiple spatial scales to compare to reported emissions. An ensemble of 30 inversions is used to quantify the uncertainty in the emission estimates.

### 2.1 Blended TROPOMI+ GOSAT methane product

The TROPOMI push-broom grating spectrometer onboard the Sentinel-5 Precursor satellite provides methane dry air column mixing ratios (XCH4) retrieved from the 2305- to 2385-nm shortwave infrared (SWIR) band and the 757- to 774-nm near-

https://doi.org/10.5194/egusphere-2025-6528
Preprint. Discussion started: 16 February 2026


infrared band. The TROPOMI XCH4 product has some residual artifacts related to surface albedo and aerosol scattering (Lorente et al., 2023). We therefore use the dataset provided by Balasus et al. (2023) who used a machine learning approach to correct the TROPOMI v02.04.00 operational product (filtered using quality assurance value = 1.0) based on the more accurate yet sparse GOSAT observations. From this point onward, the blended TROPOMI+GOSAT product will be referred to as TROPOMI and we use the original operational product in our uncertainty estimation (Section 2.9). We do not use observations along coastlines and inland waters as these data tend to have lower quality. TROPOMI observations are averaged over the GEOS-Chem resolution of 0.25° x 0.3125° as described by Estrada et al. (2025), resulting in 888987 super-observations across our domain in 2021 (Figure 1). The southern part of India has a lower observation density compared to other parts of the country due to increased cloud cover during the southwest monsoon (June to September) and the northeast monsoon (October to November) (Figure S1). The average XCH4 concentration over the Indian subcontinent for 2021 is provided in Figure 1a. The Indo-Gangetic Plain in the north shows higher methane concentrations compared to the south of India. This is primarily associated with higher methane emissions driven by anthropogenic activities, which are linked with higher population density in this region (Dangeti et al., 2024).

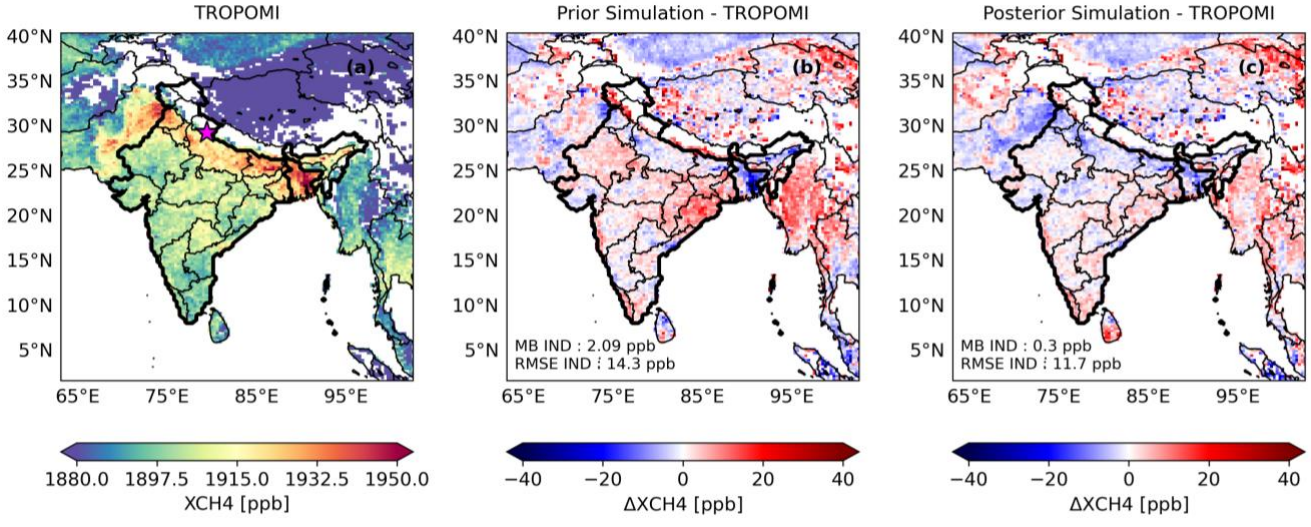


**Figure 1. TROPOMI methane dry column mixing ratios (XCH4) over India for 2021 (a). The pink star shows the location of the ground-based measurement site at Nainital. Panels (b) and (c) display the mean difference between TROPOMI observations and GEOS-chem simulations using prior and posterior emissions. Both TROPOMI data and GEOS-Chem simulations are shown at 0.25° x 0.3125°. Grid cells with fewer than 10 individual TROPOMI observations in 2021 are excluded. The mean bias (MB) and RMSE between TROPOMI and prior (b) and posterior (c) simulations are also shown. Borders are taken from Natural Earth (https://www.naturalearthdata.com/about/map-update-committee/), which provides de facto administrative boundaries.**

## 2.2 Other supporting methane observations

In addition to TROPOMI, we use facility-level emission estimates for landfills based on high spatial resolution (25x25 $m^2$) GHGSat methane data (Dogniaux et al., 2025; Maasakkers et al., 2022). The detection limit of GHGSat is ~100 kg $hr^{-1}$ for point sources; for more spread-out sources like landfills the detection limit is likely higher. Dogniaux et al. (2025) reported

https://doi.org/10.5194/egusphere-2025-6528
Preprint. Discussion started: 16 February 2026


GHGSat-based emissions from 18 different Indian landfills that have been included in this study to estimate the contribution of landfill emissions to urban emissions.

Furthermore, we use satellite and surface observations to evaluate our inversion. In January 2009, GOSAT was launched by the Japanese Space Agency (JAXA) to measure greenhouse gases (Kuze et al., 2009). GOSAT has a 13:00 local overpass time and its pixels have a diameter of 10 km, separated by about 250 km along-track and across-track (Kuze et al., 2009). Methane is retrieved using the shortwave infrared bands at 1.6 µm with the $CO_2$ proxy method, which is less sensitive to surface and aerosol related artifacts. Good methane data is obtained for about a quarter of the observations, mostly limited by cloud cover (Parker et al., 2020). We use high-quality data (quality flag = 0) from the University of Leicester Proxy GOSAT v9.0 proxy product, the same dataset used in the TROPOMI+GOSAT blended product. To eliminate the GOSAT global mean bias versus TCCON stations, 9.2 ppb is subtracted from the XCH4 data product, as suggested by Balasus et al. (2023). We also use 2021 ground-based in-situ methane measurements at Nainital (NTL) (29.36° N, 79.46° E), located at the Aryabhatta Research Institute of Observational Sciences (ARIES) (Nomura et al., 2021). Surface methane concentrations are measured weekly using the flask sampling method. Nainital, a mountain site located ~300 km away from New Delhi, can be considered a background station, although it is occasionally affected by regional-scale air pollution events.

### 2.3 Integrated Methane Inversion (IMI)

To model the relationship between emissions and TROPOMI-observed concentrations, we use the GEOS-Chem transport model as incorporated in the Integrated Methane Inversion (IMI) v1.1 framework (Varon et al., 2022) with some modifications. GEOS-Chem is a global-atmospheric chemistry transport model, with the ability to operate in nested mode at regional scale with a spatial resolution of 0.25° x 0.3125°. GEOS-Chem uses Goddard Earth Observing System Forward Processing (GEOS-FP) meteorological fields at 0.25° x 0.3125° spatial resolution and a temporal resolution of 3 hr, as provided by the NASA Global Modeling and Assimilation Office. In the methane simulation, methane removal is represented through its two major sinks: atmospheric oxidation and soil uptake. The nested version of GEOS-Chem has been applied for regional methane inversions using TROPOMI observations in various studies (e.g. Chen et al., 2022; Zhang et al., 2021). For this study, we define a nested GEOS-Chem domain encompassing India and (parts of) neighboring countries and the Indian Ocean (latitude: 1.75° N to 40.5° N, longitude: 63.125° E to 102.5° E; Figure 1). We perform simulations for 2021, using December 2020 as spin-up. Smoothed TROPOMI fields, at a spatial resolution of 2°×2.5°, are used as initial conditions and applied as boundary conditions (v2024-06) to maintain consistency with observations within the study domain (Estrada et al., 2025). Biases in the boundary conditions can result in discrepancies in the inversion process. Therefore, we optimize the boundary conditions on a yearly scale at the four domain edges and on a monthly scale for the entire domain (Section 2.5). The GEOS-Chem simulated XCH4 vertical profile is remapped to TROPOMI observations as described by Varon et al. (2022).

https://doi.org/10.5194/egusphere-2025-6528
Preprint. Discussion started: 16 February 2026


## 2.4 Prior emissions

Table 1 summarizes the prior emissions for different sectors in India. Emissions from coal, oil, and gas are taken from the Global Fuel Exploitation Inventory (GFEI v2, Scarpelli et al., 2020). Livestock, wastewater, and rice emissions are taken from EDGAR v7. Landfill emissions are also based on EDGAR v7, but for eleven Indian cities are supplemented with emission estimates for 18 landfills based on 2021–2022 GHGSat observations provided by Dogniaux et al. (2025). For these cities, the cumulative EDGAR-based landfill emissions in the 25 grid cells around the landfill are compared with GHGSat estimates. In all cases, EDGAR-summed landfill emissions are lower and are set to zero for these grids, with GHGSat emissions assigned to the grid cell containing the landfill. The "Other Anthropogenic" sector combines all remaining minor anthropogenic sources, such as road, aviation, industry, and residential emissions, based on EDGAR v7. Seasonality for each anthropogenic emission sector is applied using a scale factor derived from the monthly EDGAR v6 emission dataset. Monthly wetland emissions for 2021 are from JPL WetCHARTs (Bloom et al., 2017) at a spatial resolution of 0.5° x 0.5°. Mean emissions are calculated using the nine high-performance members of the WetCHARTs v1.3.1 ensemble, which are those members that best fit GOSAT observations (Ma et al., 2021). We also include reservoir emissions from Delwiche et al. (2022), termite emissions from Fung et al. (1991), geological seepage emissions from Etiope et al. (2019) globally scaled to 2 Tg $yr^{-1}$ (Hmiel et al., 2020), and daily open fire emissions from the Global Fire Emissions Database v4 from van der Werf et al. (2017).

**Table 1. Prior and Posterior methane emissions over India in 2021, along with the sensitivity of posterior emissions to TROPOMI data based on the inversion's averaging kernel. The sensitivity values range from 0 (no sensitivity) to 1 (full sensitivity). The values in parenthesis represent the range of inversion results derived using 30 ensemble members.**

| Sources | Prior (Tg/yr) | Posterior (Tg/yr) | Sensitivity |
|---|---|---|---|
| Total | 33.6 | 34.4 (32.0 – 40.4) | 0.6 (0.5 – 0.7) |
| Natural sources | 3.0 | 2.9 (2.4– 3.7) | 0.3 (0.2 – 0.5) |
| Reservoirs | 1.3 | 0.9 (0.7 – 1.0) | 0.3 (0.2 – 0.4) |
| Termites | 0.3 | 0.3 (0.3 – 0.4) | 0.3 (0.2 – 0.4) |
| Seeps | 0.005 | 0.008 (0.006 – 0.008) | 0.1 (0.3 – 0.6) |
| Wetlands | 1.3 | 1.6 (1.4 – 2.3) | 0.4 (0.3 – 0.6) |
| Open fires | 0.06 | 0.08 (0.04 – 0.08) | 0.4 (0.1 – 0.5) |
| Anthropogenic sources | 30.7 | 31.5 (29.6 – 36.7) | 0.6 (0.5 – 0.7) |
| Other Anthropogenic | 1.9 | 2.0 (1.9 – 2.3) | 0.5 (0.4 – 0.6) |
| Rice | 4.2 | 4.3 (3.8 – 4.8) | 0.6 (0.4 – 0.7) |
| Wastewater | 6.6 | 7.1 (6.4 – 8.3) | 0.5 (0.4 – 0.6) |
| Landfills | 1.0 | 1.3 (1.1 – 1.6) | 0.6 (0.4 – 0.8) |
| Livestock | 15.5 | 15.5 (14.0 – 18.4) | 0.5 (0.4 – 0.7) |
| Coal | 0.9 | 0.5 (0.4 – 0.64) | 0.4 (0.3 – 0.6) |

https://doi.org/10.5194/egusphere-2025-6528
Preprint. Discussion started: 16 February 2026


| | | | |
|---|---|---|---|
| Oil & Gas | 0.6 | 0.8 (0.7 – 0.9) | 0.3 (0.2 – 0.5) |

### 2.5 State vector

GEOS-Chem has a resolution of 0.25° x 0.3125°, resulting in 19,812 grid cells in our domain (Figure 1). Optimizing each grid cell as a state vector element is computationally expensive and might not be justified by the information provided by the observations. Therefore, grid cells are clustered based on proximity, number of satellite observations, and bottom-up emission estimates, following the K-means clustering method suggested by Nesser et al. (2021). This method preserves high spatial resolution for the areas with larger emission sources and higher observational density. Areas with lower emissions and insufficient satellite observations are grouped, creating larger clusters. To determine the suitable number of state vector elements, the clustering process is iterated 25 times with an increasing number of state vector elements, resulting in logarithmic growth in Degrees Of Freedom for Signal (DOFS; Section 2.6) that slows down noticeably beyond 1700 elements (Figure S2). This indicates that increasing the number of state vector elements beyond 1700 will not provide significant additional information from the inversion. To avoid the aliasing of bias into neighboring grid cells due to large clusters, clusters in the domain of interest with > 5 grids cell, an averaging kernel sensitivity >0.95, and >10 observations were split into multiple clusters. We use 1785 state vector elements, of which 1569 are located within India and 199 serve as buffer elements over neighboring countries. Additionally, 16 state vector elements are included to capture sensitivity to the background by scaling the boundary conditions (4 for the domain edges (Chen et al., 2022) and 12 for the individual months (Nathan et al., 2024)). One additional element is used to scale OH concentrations across the domain.

### 2.6 Analytical inversion

The inversion is performed with lognormal error probability density functions (pdfs) for prior emissions (Maasakkers et al., 2019). This method omits negative solutions and better captures high-tailed emissions compared to using normal errors (Duren et al., 2019; Maasakkers et al., 2022; Yuan et al., 2015). We optimize the natural logarithm of state vector $\boldsymbol{x}$, $\ln(\boldsymbol{x})$, with prior errors on $\ln(\boldsymbol{x})$ (hereafter $\boldsymbol{x'}$). For the buffer elements, boundary conditions, and OH we use normal error distributions. The Bayesian inversion method provides the optimal solution $\hat{\boldsymbol{x}}'$ to $\boldsymbol{x'}$ assuming the normal error distribution (lognormal errors for prior emission inside India) by minimizing the cost function $J(\mathbf{x}')$ (Brasseur and Jacob, 2017).

$$J(\boldsymbol{x'}) = (\boldsymbol{x'} - \boldsymbol{x'_a})^T \mathbf{S_a'^{-1}} (\boldsymbol{x'} - \boldsymbol{x'_a}) + \gamma(\boldsymbol{y} - \mathbf{K'}\boldsymbol{x'})^T \mathbf{S_o'^{-1}} (\boldsymbol{y} - \mathbf{K'}\boldsymbol{x'}) \quad (1)$$

Where $\boldsymbol{x'} = \ln(\boldsymbol{x})$ and $\boldsymbol{x'_a} = \ln(\boldsymbol{x_a})$, $\boldsymbol{x_a}(n \times 1)$ is the prior state vector estimate (n = 1785) and $\mathbf{y}$ $(m \times 1)$ contains the TROPOMI super-observations $(m = 888987)$. $\mathbf{S_a'}$ $(n \times n)$ is the prior error covariance matrix and $\mathbf{S_o}(m \times m)$ is the observational error covariance matrix. $\mathbf{K'} = \frac{\partial y}{\partial x'}$ $(m \times n)$ is the Jacobian matrix and describes the non-linear sensitivity of $\boldsymbol{y}$

https://doi.org/10.5194/egusphere-2025-6528
Preprint. Discussion started: 16 February 2026


to $\boldsymbol{x'}$. $\mathbf{K'x'} = \mathbf{Kx}$, where $\mathbf{K} = \frac{\partial y}{\partial x}$ $(m \times n)$ is the Jacobian matrix that is built by perturbing the prior emission of each state vector element by 50 %. As, a result $\mathbf{K'} = \frac{\partial y}{\partial x'}$ $(m \times n)$ can be derived using $\mathbf{k'_{i,j}} = \frac{\partial y_i}{\partial ln(x_j)} = x_j \frac{\partial y_i}{\partial x_j} = x_j k_{i,j}$ where $i$ and $j$ are the indices of the observation and state vector element. $\gamma$ is a dimensionless regularization factor and is used to avoid overfitting to the observations as $\mathbf{S_a}$and $\mathbf{S_o}$ are assumed diagonal. We estimated $\gamma$ using the L-curve analysis as described by Hansen et al. (2001), which shows that $\gamma = 0.1$ is the optimal regularization parameter (Figure S3). We also perform sensitivity tests using $\gamma = 0.05$ and 0.25 (described in Section 2.9).

The Levenberg-Marquardt method is applied to solve the non-linear problem iteratively (Rodgers, 2000).

$$\boldsymbol{x}_{N+1}{}' = \boldsymbol{x}'_N + \left(\gamma \mathbf{K}'^{\mathrm{T}}_N \mathbf{S}_o^{-1} \mathbf{K}'_N + (1+k)\mathbf{S}'^{-1}_a\right)^{-1} \left(\gamma \mathbf{K}'^{\mathrm{T}}_N \mathbf{S}_o^{-1} (\mathbf{y} - \mathbf{K}\boldsymbol{x}_N)\right) - \mathbf{S}'^{-1}_a(\boldsymbol{x}'_N - \boldsymbol{x}'_a)), \quad (2)$$

Where $N$ is the number of iterations with $\boldsymbol{x}'_0 = \boldsymbol{x}'_a$, and $\mathbf{K}'_N$ is evaluated for $\boldsymbol{x}' = \boldsymbol{x}'_N$. Equation 2 is iterated until the differences for all the state vector elements between two consecutive iterations ( $\boldsymbol{x}'_N$ and $\boldsymbol{x}'_{N+1}$ ) are smaller than 0.5 % and the $\hat{\boldsymbol{x}}' = \boldsymbol{x}'_{N+1}$ is reported as the posterior estimate. We verify that using a value of 10 for $k$ as in Chen et al. (2022) allows the optimization to smoothly converge to the posterior state and produces similar results as obtained when slowly decreasing $k$ from 100 to 0.

The posterior error covariance matrix $\hat{\mathbf{S}}'$ is derived as:

$$\hat{\mathbf{S}}' = (\gamma \mathbf{K}'^{\mathrm{T}} \mathbf{S}_o^{-1} \mathbf{K}' + \mathbf{S}'^{-1}_a)^{-1} \quad (3)$$

Where $\mathbf{K}' = \mathbf{K}'_{N+1}$ is evaluated for the posterior estimate. The averaging kernel $\mathbf{A}$ is defined as the sensitivity of the posterior solution to the true value and calculated as:

$$\mathbf{A} = \frac{\partial \hat{\boldsymbol{x}}'}{\partial \mathbf{x}'} = \mathbf{I_n} - \hat{\mathbf{S}}' \mathbf{S}'^{-1}_a \quad (4)$$

Where $\mathbf{I_n}$ is the identity matrix. A diagonal value in $\mathbf{A}$ of 0 shows that the estimation is dominated by prior information, whereas 1 indicates that observations fully inform the emission estimate. The trace of $\mathbf{A}$, defined as the DOFS, is the number of independent pieces of information on $\boldsymbol{x}'$ derived from TROPOMI observations. Applying the lognormal error distribution to the prior emissions optimizes the median instead of the mean, which are linked following $x_{mean} = x_{median} e^{\frac{\hat{s}'}{2}}$. Here, $\hat{\mathbf{S}}'$ is the posterior error covariance matrix derived using Equation 3. We report the mean emission results to facilitate comparison with inventories and include an optimization with normal error characterization in our ensemble.

### 2.7 Prior and observational error

For the emission state vector elements inside India, the prior error covariance $\mathbf{S}'^{-1}_a$ in $x'_a$ is derived from the prior emission estimates ($x_A$), assuming a 50 % uncertainty such that diagonal elements $s_A$ are $(0.5x_A)^2$. We map these uncertainties to log-normal space as described by Maasakkers et al. (2019):

https://doi.org/10.5194/egusphere-2025-6528
Preprint. Discussion started: 16 February 2026


$$s'_a = \left( \frac{\ln\left(\frac{x_A + \sqrt{S_A}}{x_A}\right) + \left|\ln\left(\frac{x_A - \sqrt{S_A}}{x_A}\right)\right|}{2} \right)^2 \quad (5)$$

This results in a lognormal prior error of 1.75. For the buffer area, we use normal prior errors of 50%. The prior error on the boundary conditions ($\sigma_{bg}$) is set to 10 ppb as in Chen et al. (2022). The prior standard deviation for OH ($\sigma_{OH}$) is 10 %. To assign equal weight to OH as the other state vector elements, the weight for the OH term is increased by taking the ratio with the total number of other state vector elements (Maasakkers et al., 2019). Super-observations are built by averaging $P$ individual TROPOMI observations at the GEOS-Chem resolution, resulting in error reduction. We use the residual error method (Heald et al., 2004) as employed by Chen et al, (2023) to determine the observation error variances for super-observation ($\sigma^2_{super}$) as:

$$\sigma^2_{super} = \sigma^2_{retrieval}\left(\frac{1 - r_{retrieval}}{P} + r_{retrieval}\right) + \sigma^2_{transport} \quad (6)$$

Where, $\sigma_{retrieval}$ is the single retrieval error covariance, $r_{retrieval}$ is the error correlation coefficient for all the TROPOMI observations averaged at the resolution of the GEOS-Chem model grid, and $\sigma^2_{transport}$ is the error covariance related to GEOS-Chem transport. Here, $r_{retrieval}$ = 0.55 and $\sigma_{transport}$ = 4.5 ppb as recommended by Chen et al. (2023) for an inversion at a resolution of 0.25° x 0.3125°, $\sigma_{retrieval}$ = 15 ppb is the standard deviation between the GEOS-Chem prior simulation and super-observations for our prior simulation, which is similar to previous studies (Nathan et al., 2024; Shen et al., 2021). Our average super-observation error variance is (11.23 ppb)$^2$ for the inversion domain, which is similar to Chen et al. (2023).

### 2.8 Emission attribution to sectors, states, and urban areas

The posterior emissions derived from the inversion method, gridded at a resolution of 0.25° x 0.3125°, can be aggregated over regions for individual source sectors using the summation matrix $\mathbf{W}$ $(p \times n)$ (Maasakkers et al., 2019). For sectoral attribution, $\mathbf{W}$ is derived by calculating the area-normalized contribution of each state vector element (n) to the corresponding source sector (p). For regional attribution, $\mathbf{W}$ represents the (area) fraction of each state vector element (n) within an assigned state or urban area (p). The reduced posterior estimates $\left(\hat{\mathbf{x}}_{\mathbf{FR,red}}\right)$, averaging kernel of the reduced system ($\mathbf{A_{red}}$), and posterior covariance $\left(\hat{\mathbf{S}}_{\mathbf{red}}\right)$ are estimated as follows:

$$\hat{\mathbf{x}}_{\mathbf{FR,red}} = \mathbf{W}\hat{\mathbf{x}}_{\mathbf{FR}} \quad (8)$$

$$\mathbf{A_{red}} = \mathbf{WAW}^* \quad (9)$$

$$\hat{\mathbf{S}}_{\mathbf{red}} = \mathbf{W}\hat{\mathbf{S}}\mathbf{W}^{\mathbf{T}} \quad (10)$$

Where, $\mathbf{W}^* = \mathbf{W}^{\mathbf{T}}(\mathbf{W}\mathbf{W}^{\mathbf{T}})^{-\mathbf{1}}$ is the Moore-Penrose pseudo-inverse of $\mathbf{W}$ (Calisesi et al., 2005) and the diagonal terms of $\mathbf{A_{red}}$ measure the ability of the inversion to estimate emissions independent of prior emissions. This attribution method assumes that grid-cell-level relative sectoral contributions to the prior are accurate and that sources are evenly distributed within the grid cells.

https://doi.org/10.5194/egusphere-2025-6528
Preprint. Discussion started: 16 February 2026


### 2.9 Error estimation and inversion ensemble

Our base inversion uses the blended GOSAT+TROPOMI product and is dependent on parameters such as the lognormal prior error $\sigma_g$ =1.75, the prior error on the boundary condition $\sigma_b$ = 10 ppb, and regularisation parameter $\gamma$ = 0.1. The posterior covariance matrix, derived using Equation 3, can represent uncertainty in the posterior estimates but does not capture the uncertainty in these parameters. To address this, we create an ensemble by varying the parameters: 1) $\sigma_g$ = 2.0, 1.75, and 1.5; 2) $\sigma_b$ = 5 ppb, 10 ppb, and 20 ppb; and 3) $\gamma$ = 0.25, 0.1, and 0.05. Additionally, sensitivity tests are conducted by using normal errors, assuming a prior error of 50%, and performing the inversion using the TROPOMI operational product. Furthermore, satellite-derived methane retrievals can be biased in case of high aerosol load (Huang et al., 2020; Somkuti et al., 2025). To mitigate these biases, a sensitivity test was conducted by excluding 63 hazy days, identified by higher aerosol optical depth (AOD) values calculated according to Bhattarai et al. (2022) and Sahu et al. (2022). These days include February 1–7, March 3–9, 14, 16, 17, 24, 29, April 3, 4, 5, 7, 30, October 21–31, and November 1 to 30. In total, we have 30 ensemble members, of which we report the range as the uncertainty on our results.

## 3 Results

We first evaluate the performance of our 2021 TROPOMI inversion over India using additional satellite and ground-based observations. Subsequently, we evaluate our results at the national, state, and urban scale and compare our estimated emissions to bottom-up inventories and estimates from the literature.

### 3.1 Evaluation of the inversion using satellite and ground-based observations

The GEOS-Chem posterior simulation demonstrates an improved fit to the TROPOMI super-observations compared to the prior simulation (Figure 1). The mean bias over India using TROPOMI super-observations decreases from 2.1 ppb to 0.3 ppb and the RMSE is reduce from 14.3 to 11.7 ppb while the correlation coefficient (r) improves from 0.89 to 0.93 (Figure S4). This indicates that the prior simulation already captures the distribution of methane over India rather well but that the inversion effectively corrects the mean bias in the emissions, while RMSE reduction is limited by the retrieval error of the individual observations. Part of the improvement is also due to the corrections to the boundary conditions. The inversion reduces the boundary condition on the southern side of the domain by 10 ppb while increasing it by 7.5 ppb on the western side (Figure S5). The monthly-scale boundary condition optimizations show a peak increase in August and a peak decrease in December (Figure S5). As shown in Figure 1, the inversion reduces overestimated methane concentrations in the prior simulation in the eastern (Odisha state), the north-western (Himachal Pradesh, Jammu and Kashmir, and Uttarakhand), and the western (Rajasthan) regions of India (A map showing all Indian states is given in Figure S6). Similar corrections are also seen over the central eastern region (Mumbai and Goa) and the southern tip (Kerala) of India. The corrections shown by the inversion are

https://doi.org/10.5194/egusphere-2025-6528
Preprint. Discussion started: 16 February 2026


more pronounced in the northern regions compared to southern regions as expected based on the higher data density and larger emissions.

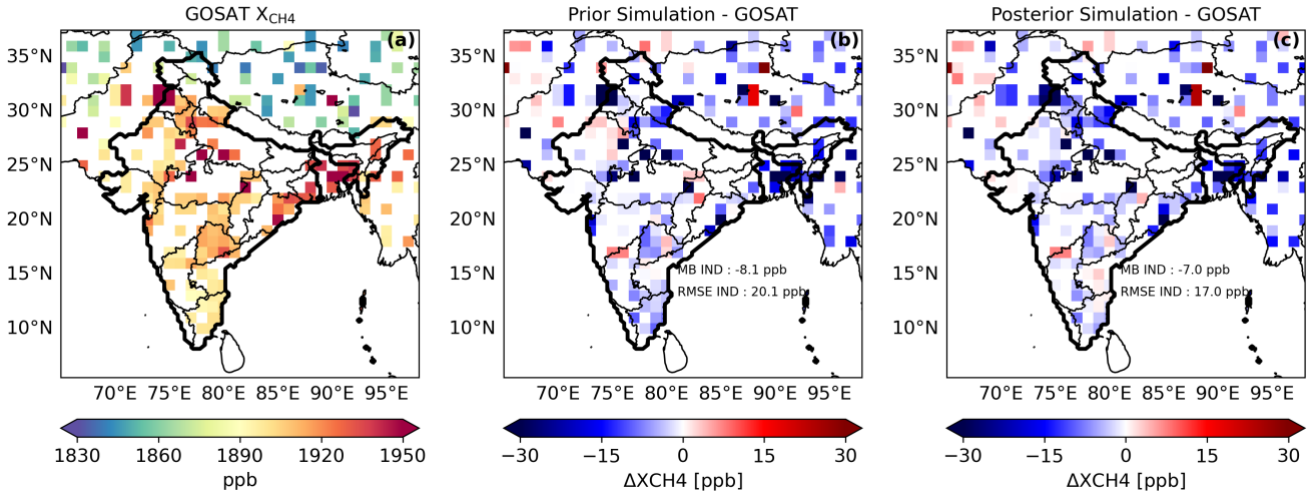


**Figure 2. 2021 GOSAT methane dry column mixing ratios (XCH4) over India (a). Panels (b) and (c) display the mean difference between GOSAT observations and GEOS-chem simulations using prior and posterior emissions, respectively. Both GOSAT data and GEOS-Chem simulations are mapped at 1.0° x 1.0° to improve visibility. Grid cells with fewer than 10 individual GOSAT observations in 2021 are excluded. Borders are taken from Natural Earth (https://www.naturalearthdata.com/about/map-update-committee/), which provides de facto administrative boundaries.**

Next, we compare the prior and posterior simulations with GOSAT observations over India (Figure 2). Despite the global correction to the GOSAT data based on TCCON, we still see somewhat larger differences between GEOS-Chem and GOSAT than compared to TROPOMI, especially over northern India. The posterior simulation shows an improved fit to GOSAT over these regions, reducing the mean bias inside India from -8.1 to -7.0 ppb, the RMSE from 20.1 to 17 ppb (which are larger than TROPOMI partly because we do not employ super-observations for GOSAT), and increasing the correlation coefficient from 0.78 to 0.87. Additionally, we find an improvement to the seasonality of the TROPOMI – GOSAT difference (Figure S7) although the differences remain larger in summer (June to August) due to limited TROPOMI coverage.

Finally, we compare our simulations to surface methane measurements at NTL (Figure S8a). The comparison shows a reduction in mean absolute error (MAE) from 73.3 ppb to 70.5 ppb. Similarly, RMSE is reduced from 88.4 ppb to 86.3 ppb. Data gaps in TROPOMI observations from March to September result in a lack of ability to correct discrepancies between NTL measurements and the posterior surface concentrations (Figure S8). Most of the realized correction is driven by observations from September to December, during which the MB improves from –7.8 ppb to 3.0 ppb (Figure S8b).

https://doi.org/10.5194/egusphere-2025-6528
Preprint. Discussion started: 16 February 2026


### 3.2 Prior and posterior emissions distributions

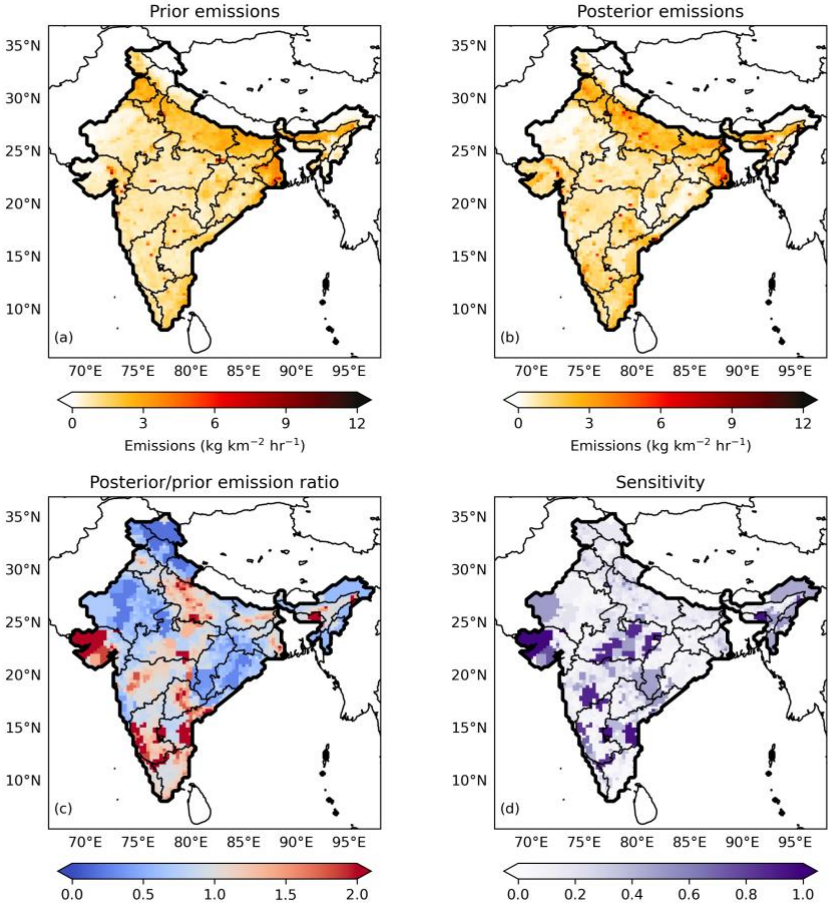


**Figure 3. Prior (a) and posterior (b) emissions from the base inversion, the ratio of posterior and prior emissions (c) and, the averaging kernel sensitivity over India for 2021 (d). Figure S9 also shows the results outside of India. Borders are taken from Natural Earth (https://www.naturalearthdata.com/about/map-update-committee/), which provides de facto administrative boundaries.**

Figure 3 shows the results from our base inversion. Although the difference between total national prior and posterior emissions is small, significant spatial variations are observed, particularly in northern (Uttar Pradesh), northwestern (Rajasthan), eastern (Odisha), and southern India (below 15N°). These regional variations are discussed in detail in Section 3.4. We find that using normal errors instead of the log-normal errors as in the base inversion produces similar correction patterns (Figure S10). However, the inversion using normal errors shows small negative emissions (- 0.4 Tg yr$^{-1}$) over several regions, which is

https://doi.org/10.5194/egusphere-2025-6528
Preprint. Discussion started: 16 February 2026


effectively mitigated using log-normal errors. The lognormal inversion tends to produce smaller downward corrections while positive corrections are larger and more concentrated in a few grid cells, consistent with the different error distributions.

The inversion provides 296 (DOFS) independent pieces of information across 1768 state vector elements. In general, averaging kernel sensitivity is higher in areas with larger methane emissions. As areas with large information density tend to be split in more state vector elements, the information content per element can be smaller there than for some larger background clusters as shown in Figure 3d.

### 3.3 National total and sectoral methane emission

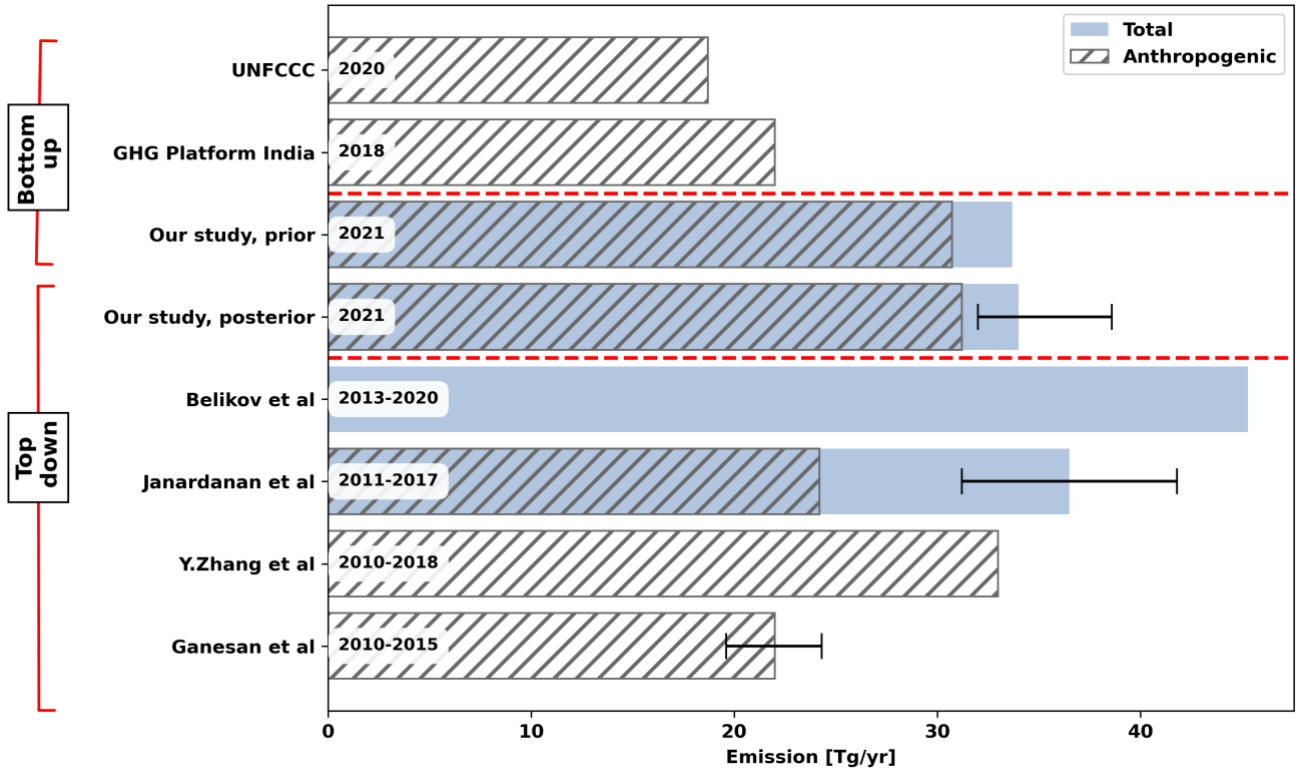


**Figure 4. Total prior and posterior methane emission over India for 2021 from our study (between dashed red lines), compared with previous bottom-up and top-down estimates representative for the years indicated in the bars. The shading shows the contribution of anthropogenic emissions to the total emission estimates; not all entries provide both total and anthropogenic emission estimates. Uncertainty ranges are reported when available, for our study they are given by the range of the inversion ensemble.**

Figure 4 presents total Indian prior and posterior methane emissions, including contributions from natural and anthropogenic sources, along with a comparison of our estimates to previous estimates. Our base inversion gives total methane emissions from India of 34.4 (32.0 – 40.4) Tg/yr, with anthropogenic sources contributing 31.5 (29.6 – 36.7) Tg $yr^{-1}$ and natural sources

https://doi.org/10.5194/egusphere-2025-6528
Preprint. Discussion started: 16 February 2026


2.9 (2.4 – 3.7) Tg $yr^{-1}$. The higher ensemble values arise from the lognormal inversion of the TROPOMI operational product, whereas lower values result from the normal inversion using the blended product. Excluding hazy days only increases the emission estimate by approximately 0.7 Tg $yr^{-1}$ compared to the base inversion, which falls within the uncertainty range. The posterior total emissions show a slight increase compared to the prior estimate of 33.7 Tg $yr^{-1}$, driven by a 3% increase in anthropogenic emissions and a 4% decrease in natural emissions, but uncertainties overlap with the prior estimates (Table 1).

Our 2021 total emission estimate aligns closely with the 2011–2017 and 2020 average total emissions of 36.6 Tg $yr^{-1}$ and 35.6 ± 0.5 Tg $yr^{-1}$, as reported by Janardanan et al. (2020) and Subramanian et al. (2025), respectively. However, a recent study by Belikov et al. (2024), which used the ground-based measurement at NTL to constrain emission over India for 2013-2020, estimated total methane emissions at 45.3 Tg $yr^{-1}$, significantly higher than our estimate. The higher estimate by Belikov et al. (2024) could be due to the local underestimation of concentrations in Nainital as also shown in our simulations (Figure S8a). Across India, however, our estimates exceed the average anthropogenic emissions reported for 2010-2015 and 2011-2017 from Ganesan et al. (2017) (22 Tg $yr^{-1}$) and Janardanan et al. (2020) (24.2 Tg $yr^{-1}$), by 43% and 30%, respectively. These differences likely arise from variation in study timeframes and higher prior emissions based on EDGAR. We also find 30% higher emissions than found for 2018-2019 by Mathew et al. (2025) (24.3 Tg $yr^{-1}$). This difference might be caused by the use of different TROPOMI retrieval products and the fact that Mathew et al. (2025) use 36 state vectors corresponding to India's political states, which are spatially extensive and exhibit complex emission source distributions. In contrast, our analysis employs 1,569 state vectors across India, enabling a more detailed representation of the spatial distribution of methane sources. In addition, Saunois et al. (2025) found that anthropogenic methane emissions over South Asia increased by approximately 9 % in 2020 compared to 2010-2019, indicating that differences in temporal coverage may partly explain the observed discrepancies.

For southern India (below 21.5 °N), our total emission estimate of 12.7 (11.4 - 15.8) Tg $yr^{-1}$ is also slightly higher than the 2017-2018 estimate from Raju et al. (2022) (10.6 Tg $yr^{-1}$) which might be due to the difference in covered time period. Compared to bottom-up anthropogenic estimates, our estimate is also substantially higher than 2020 and 2018 values reported to the UNFCCC (18.7 Tg $yr^{-1}$) and by GHG Platform India (22.0 Tg $yr^{-1}$), exceeding them by 68% and 43%, respectively. According to the GHG Platform India inventory, emissions from the energy (2.9 Tg $yr^{-1}$), industrial (0.5 Tg $yr^{-1}$), and biomass burning in forests and croplands (0.31 Tg $yr^{-1}$) together account for approximately 17% of total anthropogenic methane emissions, while livestock, rice and waste contribute the remaining 83 %.

https://doi.org/10.5194/egusphere-2025-6528
Preprint. Discussion started: 16 February 2026


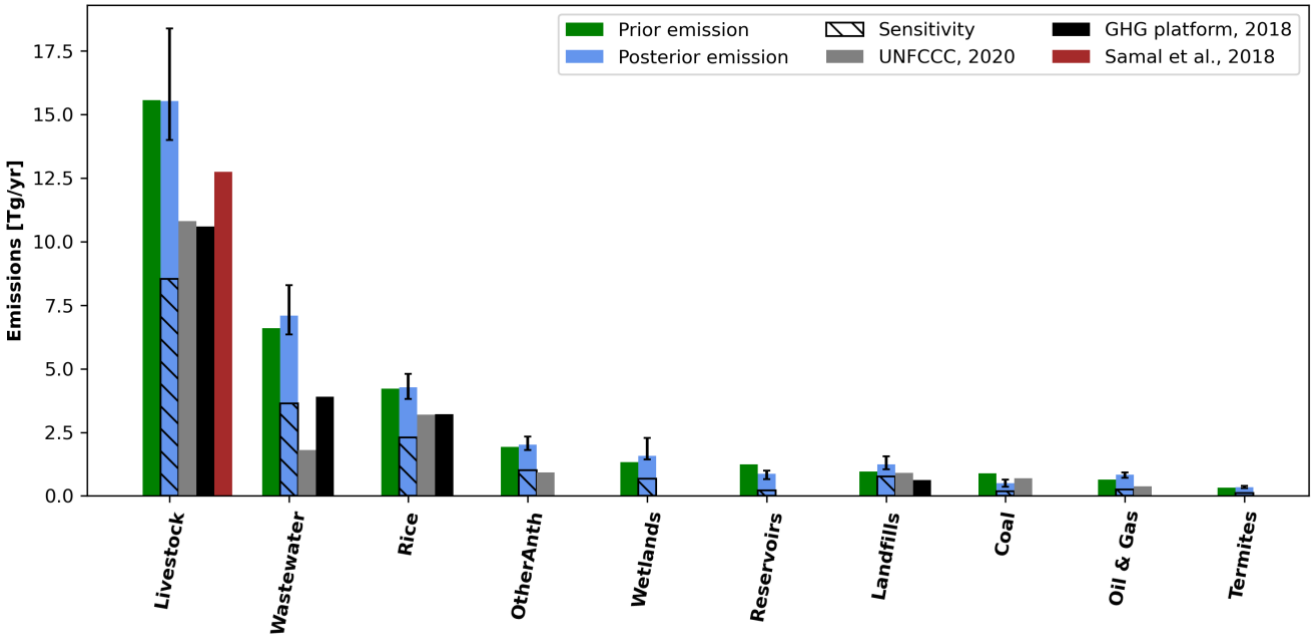


**Figure 5. Prior and posterior emissions derived from the inversion shown for different sectors over India in 2021 and comparison to bottom-up inventories. The error bars represent the ensemble range. The sensitivity for each sector is derived using the averaging kernel, shown as hashed bars that cover a fraction of the emission bars. These sensitivities are a measure for the extent to which the posterior emission estimates are constrained by the satellite observations. For the GHG Platform comparison, only sectors whose definitions are consistent with our source categories are included in the figure.**

To understand these differences, we allocate national total emissions to emission sectors following the attribution procedure described in Section 2.8. The sectoral prior and posterior emissions, along with sensitivity, are presented in Figure 5. Livestock, wastewater, rice, and landfill emissions contribute 82 % of posterior emissions and TROPOMI strongly constrains these four sectors with averaging kernel sensitivities between 0.5 and 0.62. For other sectors, the averaging kernel sensitivity ranges between 0.3 and 0.5. The posterior correlations between individual sectors are derived using the off-diagonal elements of $\hat{S}_{k,red}$ (Equation 10). Among the major emission sources, we do observe higher correlations (r>0.5) between livestock, wastewater, rice, and other anthropogenic sources because of their similar spatial distributions (Figure S11). In contrast, correlations among the other sources are generally below 0.5 (Figure S11).

The livestock posterior emission shows a small change compared to the prior and is estimated at 15.5 (14 – 18.4) Tg $yr^{-1}$. This value is slightly higher than the 12.8 Tg $yr^{-1}$ reported for 2018 by Samal et al. (2024), who used livestock activity data from 1992-2019 provided by the Indian government, along with modified emission factors derived by averaging the IPCC-2006 emission factors and the 2004 National Communication (NATCOM) emission coefficients (MOEFCC, 2004) assigned to different livestock age groups. Meanwhile, the UNFCCC inventory and GHG platform India report livestock methane emissions of 10.8 Tg $yr^{-1}$ and 10.6 Tg $yr^{-1}$ , both lower than our posterior and prior emissions as well as Samal et al. (2024).

https://doi.org/10.5194/egusphere-2025-6528
Preprint. Discussion started: 16 February 2026


The UNFCCC and GHG platform India calculations use NATCOM and IPCC Tier I and II based emission factors rather than the modified emission factor used by Samal et al. (2024) and rely on 2019-2020 livestock activity data indicating ~539 million heads of cattle in India. In contrast, EDGAR emissions are derived using IPCC default emission factors, leading to discrepancies when compared to the UNFCCC, GHG platform India, and Samal et al. (2024) estimates (Regional differences are further analyzed in Section 3.4). Overall, these differences are likely due to temporal variations, discrepancies in activity data, and differences in emission factors, as due to small herd sizes and lack of industrialization, local emission factors are relatively low (Shahid et al., 2024). We estimate rice emission of 4.3 (3.8 – 4.8) Tg $yr^{-1}$ within the uncertainty range of Ganesan et al., (2017) (~3.9 (3.3–4.5) Tg $yr^{-1}$) , which are 34% larger than the UNFCCC and GHG platform India estimate. Rice emissions may be higher because of low rates of mechanized agriculture and heavy dependence on flood-based cultivation with two growing seasons (Dong et al., 2006).

Landfill and wastewater emissions increased by 31% and 8% compared to the prior estimates. These increases are particularly concentrated in cities, which are further examined in Section 3.5. UNFCCC-reported landfill emissions are 0.9 Tg $yr^{-1}$, slightly lower than our estimate, while GHG platform solid waste emissions are lower by a factor 2. Wastewater emissions (7 Tg $yr^{-1}$) are higher than estimated by the UNFCCC inventory and GHG platform India by factors 3.9 and 1.8, respectively. The higher posterior wastewater emissions may be attributed to the higher prior EDGAR emissions, which could be aliasing emissions from other urban sources including landfills into the wastewater category. This could especially happen for cities where we did not have GHGSat data to improve the spatial allocation of landfill emissions, which would leave the spatial pattern very similar to wastewater treatment and make it impossible for the inversion to distinguish emissions from the two sources.

The posterior emissions for the oil & gas sector are 0.8 Tg/yr, higher by 30% compared to the prior (0.6 Tg $yr^{-1}$), mainly due to increased emissions in northeastern India and West Bengal. The UNFCCC-reported oil & gas methane emissions are 0.4 Tg $yr^{-1}$ and the report mentions that leakage from vents and undocumented flaring contributes to higher uncertainty on the emission estimates (MoEFCC, 2024) . High-resolution GHGSat observations have previously shown the presence of large site-level methane super-emitters in the northeast of India (Schuit et al., 2023), supporting the hypothesis that these could cause a difference between reported and observed methane emissions. We observed significantly lower (57%) coal emissions than included in the prior estimate, consistent with the UNFCCC estimate within our uncertainty range. Similar reductions in coal emissions of ~50 % are observed over the eastern part of India and West Bengal (Regional patterns are further examined in Section 3.4). Reservoir posterior emissions decreased by 31% compared to the prior. Additionally, wetland emissions increased by 18 %, particularly in southern India, Bihar, and Gujarat.

https://doi.org/10.5194/egusphere-2025-6528
Preprint. Discussion started: 16 February 2026


### 3.4 State emissions

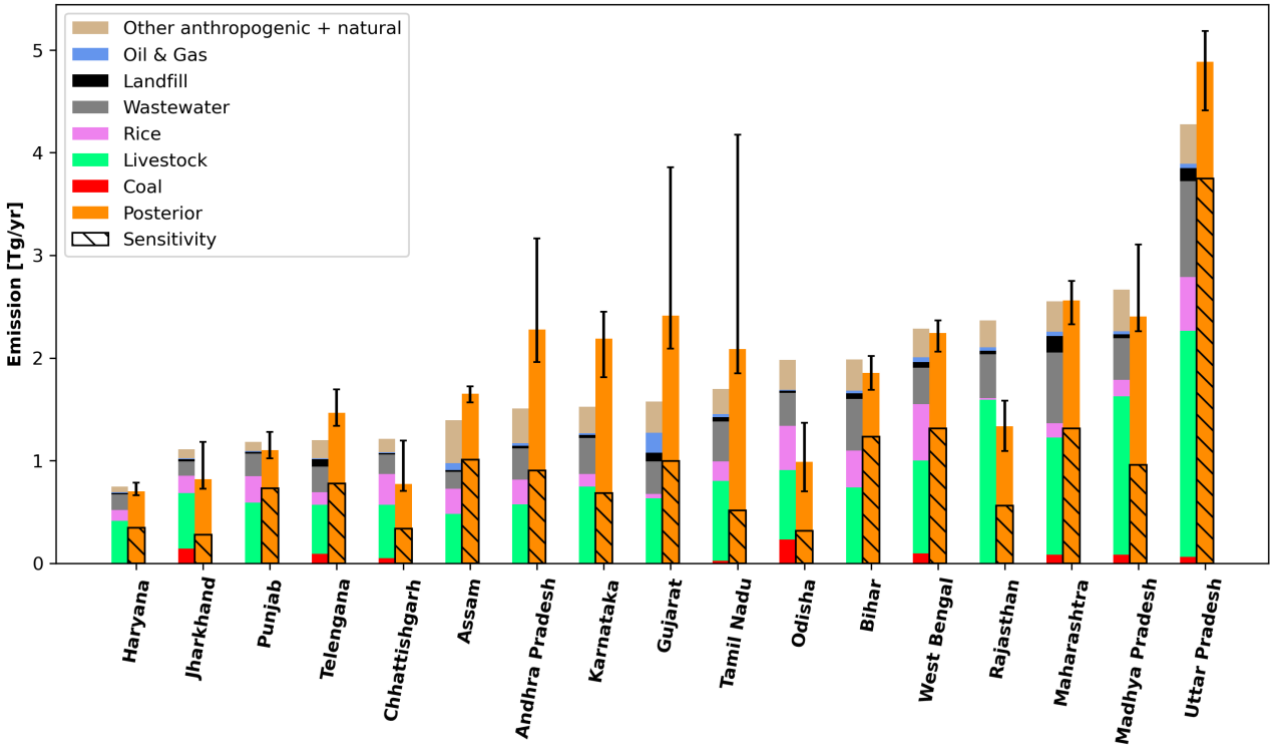


**Figure 6. Prior emissions with sectoral contributions and posterior emissions derived across the 17 states in India with prior emissions above 0.6 Tg/yr. A map with state names is given in Figure S6. Error bars show the range of the 30-member ensemble. The sensitivity for each state is derived from the averaging kernel, represented by bars with hashed patterns shown as a fraction of the emissions. These sensitivities are a measure for the extent to which the posterior emission estimates are constrained by the satellite observations.**

To understand regional-level methane emissions, we analyze the 17 Indian states with prior emissions above 0.6 Tg $yr^{-1}$ as shown in Figure 6. Total prior and posterior emissions are calculated by summing grid cells within the state boundaries and the averaging kernel sensitivities are derived as described in Section 2.8. Among all the states, Uttar Pradesh has the highest posterior methane emissions followed by Maharashtra and Madhya Pradesh. The uncertainties on the posterior emissions are based on the ensemble, with higher values typically driven by the members using the TROPOMI operational product. Tamil Nadu has the lowest sensitivity (0.3) due to lower observation density and a lack of significant TROPOMI-observed enhancement, which also results in a wide uncertainty range. The posterior emissions for the other 16 states are well constrained by TROPOMI with sensitivity values ≥0.4. Among the 17 states, nine show significant differences between prior and posterior emissions. Among them, seven show increases in posterior emissions ranging from 14% to 54%, with Karnataka, Gujarat, and Andhra Pradesh showing increases by more than 40%. These larger increases are mainly due to waste and livestock in Andhra Pradesh and Karnataka, and the oil & gas sector in Gujarat. Two states exhibit significant reductions; posterior emissions are

https://doi.org/10.5194/egusphere-2025-6528
Preprint. Discussion started: 16 February 2026


44% lower for Rajasthan and 50% lower for Odisha (Table S1). In general, this suggests relatively large uncertainties in bottom-up inventories at the state level.

We also compare our posterior livestock, landfill, and wastewater emissions with the independent bottom-up estimates provided by GHG platform India. In all states except Odisha, livestock contributes over a third of prior emissions, with the highest emissions in Uttar Pradesh and highest contribution in Rajasthan (67 %, Figure S12a). Across all states, more than 90% of livestock methane emissions reported by the GHG Platform are attributed to enteric fermentation, for which cattle and buffalo are the primary contributors (MoEFCC, 2024). The cattle and buffalo population data used by the GHG Platform and EDGAR are similar; however, their emission factors differ: the GHG Platform uses emission factors from India's NATCOM (MOEFCC, 2004), while EDGAR relies on IPCC default values. The IPCC emission factor for dairy indigenous cattle (46 kg $head^{-1}$ $year^{-1}$) is approximately twice as high as the value used in NATCOM (28 ± 5 kg $head^{-1}$ $year^{-1}$), resulting in discrepancies between EDGAR and GHG Platform livestock emission estimates. The posterior emissions reveal regional variations, including increases in methane emissions over Uttar Pradesh, Gujarat, and southern India. Unlike coal and natural gas, the more spread-out livestock emissions do not feature clear regional hotspots that we can use to draw definitive conclusions about sector-specific trends from the inversion results.

The GHG Platform India estimates waste sector emissions using secondary data sourced from several national sources and employing Tier 1 and Tier 2 methodologies, incorporating country-specific and state-level emission factors. EDGAR, on the other hand, uses the IPCC Waste Model and distributes emissions spatially based on population. Differences in both activity data and emission factors can therefore lead to variations between the two estimates**.** Both our posterior and GHG platform India emissions show that Uttar Pradesh and Maharashtra have the highest total waste-related methane emissions (Figure S12b and c). Landfill emissions are consistent between prior and posterior in two states (Andhra Pradesh and Karnataka) but vary elsewhere. Except for Punjab, GHG platform India's wastewater emissions are lower by 34% to 265% compared to our posterior estimates. This difference is most likely due to the higher prior values from EDGAR, which could have masked emissions from other urban sources, resulting in sectoral misattribution. Urban waste emissions are discussed in detail in Section 3.5.

Coal mining methane emissions are highest in Odisha and Jharkhand, the largest coal producers in the country. Both states show reduced posterior emissions. At the Talcher coal field in Odisha (20.977° N, 85.137° E), which holds India's largest geological coal reserves (Panda et al., 2022), posterior emissions are lower by a factor 6.5, reducing them from 26.3 tons/hr to 4.1 (3.0–6.2) tons/hr. Coal production has been expanding largely through surface mining, which is generally not as methane intensive as underground mining. If this shift is not reflected in activity data, this could lead to overestimated bottom-up emission estimates (Wright et al., 2024). Oil & gas activities are strongly concentrated in Assam. The Assam oil and gas field

https://doi.org/10.5194/egusphere-2025-6528
Preprint. Discussion started: 16 February 2026


(27.39° N, 95.43° E), one of the oldest fields in India, previously identified as a super-emitter based on TROPOMI by Schuit et al. (2023), shows a factor 2.4 increase in posterior emissions, from 3.3 tons/hr to 8.0 (7.0 - 8.3) tons/hr. This estimate is based on the sum of emissions from 25 surrounding grid cell and falls within the uncertainty range of the sum of site-level emissions reported by Schuit et al. (2023) at 12.9 ± 4.3 tons/hr based on a GHGSat observation from December 24, 2024, suggesting that a large fraction of emissions could come from a limited number of strongly emitting sites. Increasingly complex extraction due to declining production levels, difficult terrain, and aging infrastructure as well as several large-scale blowouts, could explain increased methane emissions (Goswami and Ghosh, 2021; Guha, 2025; Mohanty and Dutta, 2023).

### 3.5 Urban emissions

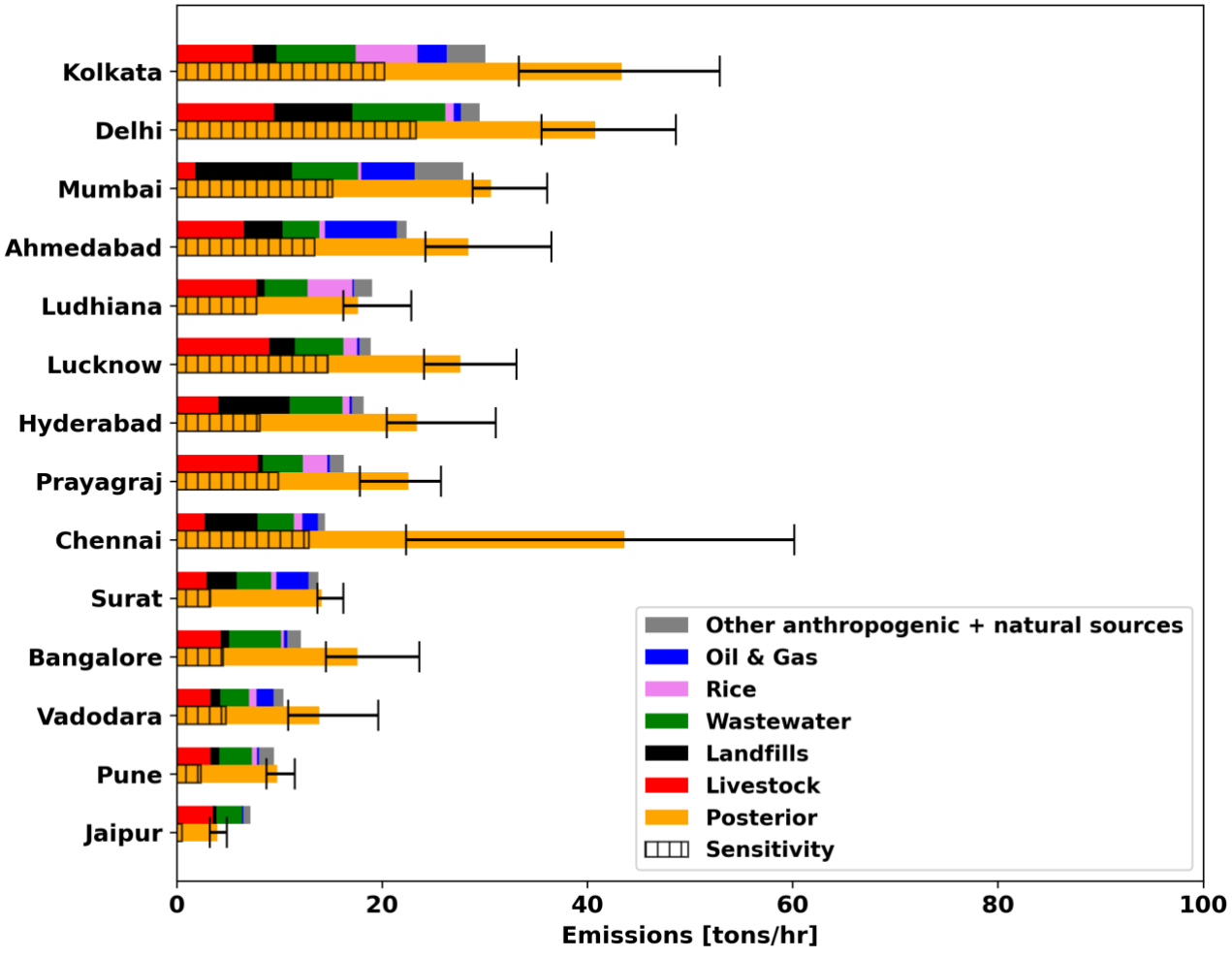


**Figure 7. Comparison of prior emissions with sectoral contributions and posterior emissions derived across 14 Indian cities. Total prior and posterior emissions are calculated as the cumulative sum of emissions across nine grid cells surrounding each city center. Error bars represent the uncertainty derived from the 30-member ensemble. The sensitivity for each city is derived from the**

https://doi.org/10.5194/egusphere-2025-6528
Preprint. Discussion started: 16 February 2026


**averaging kernel, represented by bars with hashed patterns shown as a fraction of the emissions. These sensitivities are a measure for the extent to which the posterior emission estimates are constrained by the satellite observations.**

We further analyze our results over 14 cities (Figure 7). To do so, we compare the cumulative prior and posterior emissions in the 9 model grid cells around the center of each city. Among these cities, Kolkata has the highest prior methane emission estimate followed by Delhi and Mumbai. The breakdown of prior emissions shows a large variety of sources contributing. The emission breakdowns discussed here are based on mapped bottom-up inventories (mainly EDGAR v7), supplemented with GHGSat data for landfills. These come with significant uncertainty, and the resulting urban estimates are not always in agreement with local greenhouse gas inventories, as for example compiled by cities. Some of the cities also include some emissions from activities around the city center, such as rice cultivation near the Hooghly River for Kolkata and livestock in Delhi. Methane emissions from waste (landfill + wastewater) contribute 30% to 70% of total urban methane emissions. The analyzed cities represent different tiers of India's urban hierarchy, waste management maturity, and waste monitoring (Kumar et al., 2017). Metropolitan cities are governed by municipal corporations with dedicated waste departments, while some others have seen a rapid expansion of solid waste management capacity under Swachh Bharat Mission-Urban initiatives (Zhu et al., 2012). EDGAR landfill and wastewater emissions generally show a strong spatial correlation ($r > 0.9–1.0$) across cities. After incorporating GHGSat emission estimates into our prior emissions for 11 cities, the correlation between landfill and wastewater emissions decreases to a range from 0.1 to 0.8. Higher correlations ($r = 0.7–0.8$) are observed in cities such as Mumbai and Delhi, where multiple landfills are present and GHGSat-based emissions therefore more closely align with the population-based spatial allocation of EDGAR wastewater emissions. Overall, the incorporation of GHGSat-based landfill emissions improves the ability of our inversion to distinguish solid waste and wastewater emissions (Figure S11). Landfills are the largest source in Mumbai, Hyderabad, and Chennai, while wastewater is the largest source in Surat, Pune, and Bangalore. The landfill dominance in major cities reflects both current waste generation volumes and the historical legacy of dumping (Ravish, 2025), with cities like Mumbai (Deonar, Mulund) and Delhi (Okhla, Ghazipur, Bhalswa) having landfills that have received decades of waste (Express, 2025). Under the Solid Waste Management Rules 2016, all states were mandated to investigate and remediate legacy dumpsites through bio-mining and bioremediation, yet many cities continue to have active dumpsites alongside newer engineered facilities (CPCB, 2019). The 2024 Draft Solid Waste Management Rules, which mandate treatment of at least 90% of waste by 2027, reflect the evolving policy landscape.

For cities with relatively large emissions, the sensitivity values of the inversion are around or above 0.5, indicating emissions are well informed by the TROPOMI observations (Table S2). Jaipur has the lowest information content due to its smaller size and lack of prominent enhancement in TROPOMI data. In Surat, Pune, and Ludhiana, prior and posterior estimates are closest while posterior emissions in Chennai show the largest increment (factor 3) compared to prior estimates. As Chennai is a coastal city, it is more difficult to observe with TROPOMI, resulting in a larger uncertainty range compared to other cities. For nine other cities, posterior emissions are 10 to 50% higher than prior estimates (Table S2), indicating a general tendency for the used bottom-up inventories to underestimate urban emissions. Comparing our estimates to previous studies, we find that our

https://doi.org/10.5194/egusphere-2025-6528
Preprint. Discussion started: 16 February 2026


estimates for Mumbai and Delhi are consistent with the TROPOMI inversions using the WRF model by Maasakkers et al. (2022). Foy et al. (2023) estimated emissions for seven of the studied cities, finding estimates that are larger by factors of 1.4 to 3.6 compared to our posterior estimates. They noted that such discrepancies were also observed when comparing their estimates with those of Maasakkers et al. (2022) and attributed them to differences in how wind speed and boundary layer conditions were applied in the respective studies and the fact that their approach required Gaussian-shaped urban enhancements.

The discrepancies between observations and bottom-up estimates could be significantly affected by unreliable activity and emission factor data, both in terms of what is available and what is incorporated in EDGAR. Cities do generally not have historical or updated waste composition data and rely on extrapolations and interpolations for the contents of the landfill. Both activity data and emission factors are expected to vary by city, site, and season, and site-level practices are difficult to capture in bottom-up inventories (Singhal et al., 2022). Substantial portions of waste in Indian cities pass through informal waste pickers and recyclers, meaning reported waste quantities often underestimate the total material streams entering disposal sites (Simpson et al., 2025). Furthermore, hazardous and sanitary waste can overlap, combined with scavenging and bioremediation activity where older buried waste is excavated, leading to heterogeneous and complex methane generation patterns (Priya and Gupta, 2019). Under Swachh Bharat Mission-Urban and subsequent initiatives (MoHUA, 2021), many cities have expanded biomethanation and waste-to-energy capacity, yet these facilities often show slower operational ramp-up than planned and operational challenges can prevent effective emission reduction (Ahluwalia and Patel, 2018). While cities like Bangalore, Pune, and Hyderabad have relatively advanced waste management infrastructure (Hamdan et al., 2025), they show larger emissions than included in the (generic) EDGAR inventory.

Foy et al. (2023) posed that untreated wastewater is a major contributor to methane emissions in seven studied Indian cities and that these emissions could be reduced by 50% with wastewater treatment plants. Our prior emissions indicate that wastewater contributes 20% to 35% of total methane emissions across the 14 cities. In Mumbai, Surat, Pune, and Ludhiana, posterior and prior wastewater emissions are similar. Chennai shows the largest increase by a factor 2.9, while for the other eight cities posterior emissions are higher by 33% to 58%, suggesting underestimation in the bottom-up emission estimates. Bottom-up calculations, which typically rely on treatment-facility data, can substantially underestimate emissions by missing emissions from distributed open defecation alternatives and informal waste treatment (Singh, 2023). The absolute increase in posterior wastewater emissions correlates with the proportion of the associated urban populations lacking wastewater facilities ($r=0.4$). Furthermore, cities where posterior emissions are more than 35% higher than the prior, align with cities for which Climate TRACE data shows that >40 % of the population lacks access to wastewater treatment (Figure S14). Many cities lack primary or secondary treatment facilities, with wastewater either flowing directly into water bodies or being treated through rudimentary methods that do not capture methane emissions (NITI Aayog, 2022). Among all cities, Kolkata and Delhi have the highest posterior wastewater emissions, consistent with Climate TRACE data showing that 90 % and 60 % of their

https://doi.org/10.5194/egusphere-2025-6528
Preprint. Discussion started: 16 February 2026


populations lack access (Figure S14). Kolkata's Hooghly River receives substantial untreated sewage from sprawling informal settlements, while Delhi's wastewater infrastructure, despite recent investments, remains inadequate for the city's growing population (Guptha et al., 2021; Rajan et al., 2023). In contrast, for Mumbai and Surat, where prior and posterior wastewater emissions are similar, Climate TRACE reports that more than 95% of the population has access to wastewater treatment plants.

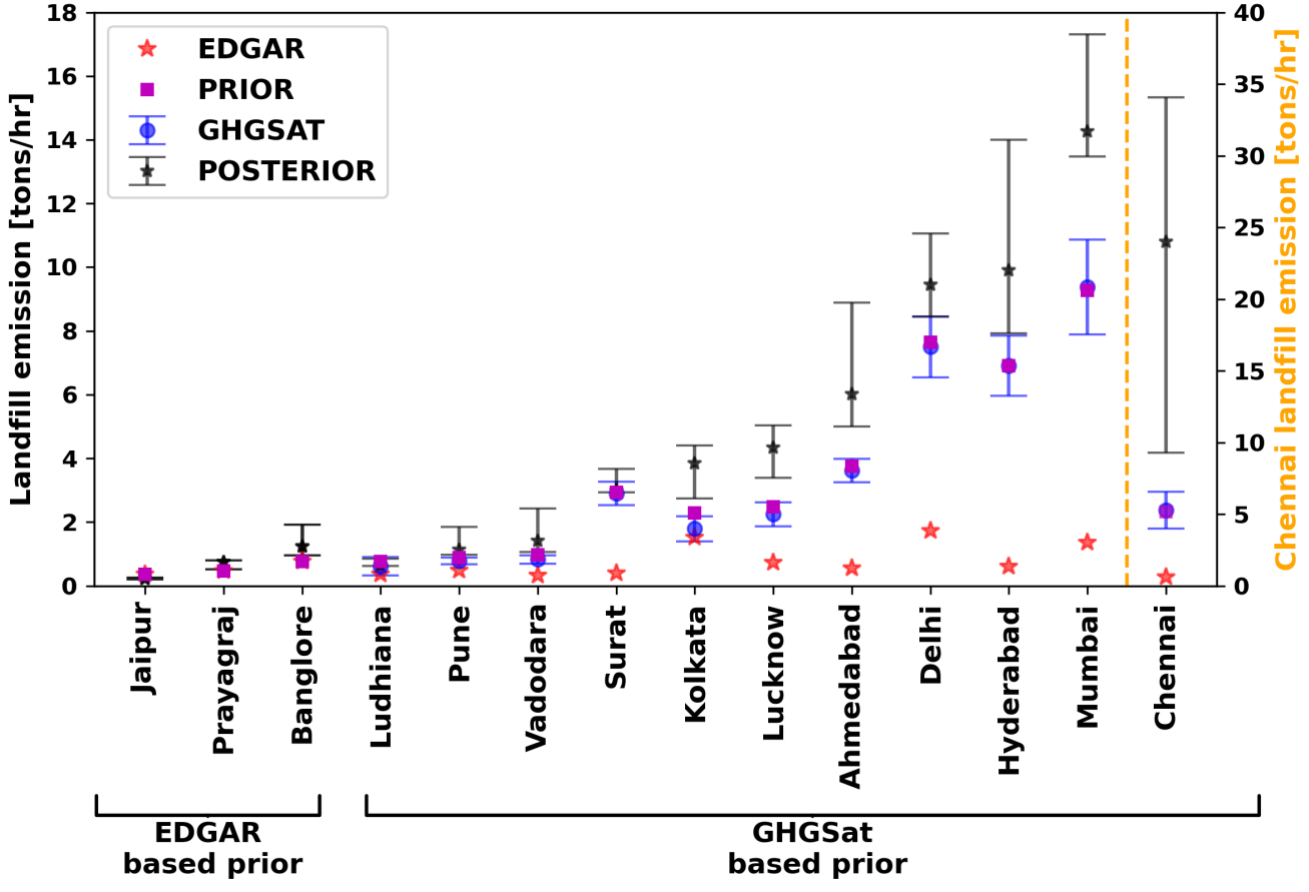


**Figure 8. Landfill emissions across 14 cities derived from EDGAR and GHGSat, and the posterior emission estimates. The prior landfill emissions used in the inversion are based on EDGAR for the first three cities, while for the remaining 11 cities, they are based on GHGSat (as described in Section 2.4). The total prior, total posterior, and total EDGAR landfill emissions (indicated with a star) are calculated by summing emissions across nine grid cells (0.25° x0.3125°) surrounding each landfill. The error bars represent the uncertainty estimates derived from the 30-member ensemble.**

Figure 8 shows landfill emissions obtained from EDGAR, GHGSat, and the TROPOMI inversions (Table S3). Among the cities for which we have GHGSat data, Delhi has four observed landfills, while Chennai, Mumbai, Kolkata and Lucknow have two. These cities often have multiple landfills within one model grid cell, limiting our ability to compare posterior emissions to GHGSat estimates directly. We therefore compare total prior, posterior, and EDGAR-based landfill emissions derived by

https://doi.org/10.5194/egusphere-2025-6528
Preprint. Discussion started: 16 February 2026


summing emissions across nine model grid cells (0.25° x0.3125°) surrounding each landfill. Among the three cities with EDGAR-based prior emissions, posterior landfill emissions in Bangalore and Prayagraj are higher by a factor of 1.6, while the estimate for Jaipur remains close to EDGAR as the city is poorly informed by observations (Figure 7). As the prior landfill emissions in the other 11 cities incorporate GHGSat-derived emissions, total prior and GHGSat landfill emission estimates generally match. In these 11 cities, both GHGSat-based and posterior emission estimates are all higher than the EDGAR-based landfill emissions, with significant differences for seven of the cities. This suggests that EDGAR-based landfill emissions are underestimated, possibly because the inventory lacks site-level landfill data. Our posterior emission estimates generally match well with the GHGSat emissions, though they are not fully independent because of the incorporation of GHGSat estimates in the prior. Many of the cities studied here have more waste sites than were observed by GHGSat. The Climate TRACE data show that Chennai has 23 dumping sites (including the two GHGSat-observed locations), the most among all the cities (Figure S13). Similarly, Hyderabad, Mumbai, Ahmedabad, and Lucknow have 12, 10, 8, and 2 additional dumping sites, respectively. This reflects India's fragmented waste management landscape, where most metropolitan areas do not have single, centralized disposal facilities but rather operate multiple active dumpsites managed by different parties alongside legacy closed dumpsites undergoing remediation. Smaller and informal dumpsites often go unmonitored in official inventory systems. However, the landfills that GHGSat observed are the largest in terms of area, contributing ≥ 80 % of the total landfill area in each city (Figure S13). Still, the numerous additional smaller dumping sites can contribute to total emissions, potentially leading to differences between GHGSat and posterior estimates for those cities. The coastal city of Chennai has the highest posterior methane emission estimate, as it shows a high methane enhancement in TROPOMI that leads the inversion to scale up all sources, including landfills.

## 4. Conclusion

India is one of the top global emitters, with a large population, rapidly growing economy, and complex policy environment. This makes the quantification of methane emissions across spatial and policy scales key to enable efficient mitigation of emissions. In this study, we estimated India's methane emissions for 2021 using the blended TROPOMI+GOSAT methane data in an inversion with the GEOS-Chem model at a resolution of up to 0.25° x0.3125°. We used prior emissions based on GFEI v2 and EDGAR v7, supplemented with site-level GHGSat estimates for 18 landfills. Posterior emissions were derived using an analytical Bayesian inversion method with log-normal errors on emissions and ensemble-based uncertainty estimates. The inversion shows improved agreement with TROPOMI observations as well as with GOSAT and surface-based observations. The high resolution of the inversion and incorporation of facility-level GHGSat data enable us to use the inversion to estimate emissions across spatial scales and compare with a range of policy-relevant existing emission estimates.

The total posterior methane emissions for India are 34.4 (32–40.4) Tg $yr^{-1}$, a value comparable to recent studies by Janardanan et al. (2020) and Subramanian et al. (2025). Anthropogenic posterior emissions are 31.5 (29.6 – 36.7) Tg/yr, close to our

https://doi.org/10.5194/egusphere-2025-6528
Preprint. Discussion started: 16 February 2026


EDGAR/GFEI-based prior but 68% higher than UNFCCC-reported values. Zhang et al. (2021) found a similar difference of 75%, while smaller discrepancies of 17-30 % have been observed by Ganesan et al. (2017), Janardanan et al. (2020), and Mathew et al. (2025), potentially due to differences in covered time period, prior emissions, and inversion methodology. Our sectoral breakdown of posterior emissions shows that most anthropogenic sources can be independently estimated with large adjustments to landfill emissions (+30%) and oil & gas (+33%) emissions, while coal emissions are found to be lower (-56%).

Analyzing methane emissions from the 17 states with the largest emissions, we find strong regional discrepancies with inventories that are strongly informed by TROPOMI data except for one state with limited observational coverage. Inversion results show significantly higher emissions in seven states with corrections up to 52% compared to the prior estimates. Notable increases can be related to oil & gas in Assam and Gujarat. Two states show significantly lower emissions than included in the prior, with Odisha (-52%) showing the largest decrease, primarily due to lower coal mining emissions. We also compared state-wise posterior estimates for livestock, wastewater, and landfill emissions with state-level emissions reported by the GHG platform India, generally finding higher estimates for all sources.

Finally, we analyzed urban methane emissions in 14 cities, where waste-related sources (landfills and wastewater) dominate. In nine cities, posterior emissions are 10% – 50 % higher than the prior estimates, while in Chennai they increase by a factor of three, indicating that the used bottom-up inventories tend to underestimate urban emissions. Incorporating GHGSat landfill emissions in our prior emission estimates improved the ability of our inversion to separate landfill and wastewater emissions. While EDGAR landfill and wastewater emissions were initially highly correlated ($r > 0.9$), the correlation decreased after including GHGSat data, reflecting better source separation. We find significantly higher posterior wastewater emissions for nine cities and find that the absolute increase in posterior wastewater emissions correlates ($r=0.4$) with the fraction of urban population lacking access to wastewater treatment facilities. Kolkata and Delhi have the highest wastewater emissions, consistent with Climate TRACE data showing that 90% and 60% of their populations lack access. Among the 14 cities, 11 have GHGSat observations, which indicate that landfills contribute 10–38% of posterior urban methane emissions, underscoring the importance of solid waste management in reducing methane emissions. It also illustrates that urban waste emissions are poorly captured by currently available gridded inventories, calling for bottom-up emission estimates capturing the complex and heterogeneous emissions from individual solid waste disposal sites.

Despite providing valuable insights into methane emissions across multiple spatial scales, this study has some limitations. Sectoral attribution remains strongly dependent on the prior emission source distribution, creating uncertainty in sector-specific estimates. Incorporating facility-scale landfill observations improves prior estimates, further integration of country-specific information in gridded inventories, along with additional facility-scale (observational) data for sectors such as oil & gas and coal, could substantially enhance the quality of prior estimates and the associated inversion results. Validation of the inversion results is limited to GOSAT observations and a single in situ measurements site, which constrains the assessment of model

https://doi.org/10.5194/egusphere-2025-6528
Preprint. Discussion started: 16 February 2026


performance. The information content and evaluation of future inversion results could be substantially improved through comprehensive and systematic in situ methane monitoring across the country. In addition, this analysis is limited to a single year, as extending the inversion to multiple years is computationally intensive. Consequently, the assessment of seasonal variability and interannual trends in methane emissions and their sectoral drivers remains limited. More extensive TROPOMI observations and analysis in the future can enable a more comprehensive evaluation of temporal changes and a deeper understanding of emission drivers and their seasonal dynamics.

Overall, this study emphasizes the critical role of top-down approaches that combine multiple satellites in evaluating bottom-up emission estimates. This spatially explicit analysis can inform subnational prioritization and guide follow-up investigation and capacity building (e.g., observation campaigns, activity data gathering, and inventory refinement) and support the development of effective methane mitigation strategies. The incorporation of facility-scale data and our approach for evaluation across spatial scales can readily be extended to other countries.

**Data availability**

The operational TROPOMI product is available at: https://dataspace.copernicus.eu. The blended TROPOMI+GOSAT product is available at: https://registry.opendata.aws/blended-tropomi-gosat-methane. The ground-based observations are available at: https://www.nies.go.jp/doi/10.17595/20220301.003-e.html. GHGSat data for landfills are available at: https://doi.org/10.5281/zenodo.16641833. GOSAT data is available at: https://dx.doi.org/10.5285/18ef8247f52a4cb6a14013f8235cc1eb. GHG platform data is available at: https://www.ghgplatform-india.org. The surface station data are available through https://www.aries.res.in/research/atmospheric-science. The IMI code can be access from https://github.com/geoschem/integrated_methane_inversion.

**Author contributions**

SL and JDM developed the conceptual ideas for the study. SL performed the analysis and wrote paper with input from JDM and IA. XZ, SD, and SN contributed to the interpretation of the results and compilation of the paper. DJV, MPS, and LE supported the IMI analysis. NB provided TROPOMI+GOSAT blended data. MG supported the interpretation of the GHGSat data. RP supported the use of the GOSAT data. YT provided ground-based data over Nainital. All co-authors commented on the paper and improved it.

**Competing interests**

The authors declare that they have no conflict of interest.

https://doi.org/10.5194/egusphere-2025-6528
Preprint. Discussion started: 16 February 2026


**Acknowledgements**

This work was funded by the Targeting Waste emissions Observed from Space (TWOS) project funded by the Global Methane Hub. We thank the team that realized the TROPOMI instrument and its data products, consisting of the partnership between Airbus Defense and Space Netherlands, KNMI, SRON, and TNO and commissioned by NSO and ESA. The Sentinel-5 Precursor is part of the EU Copernicus program, and Copernicus (modified) Sentinel-5P data (2021) have been used. The authors acknowledge the support of SURF Cooperative, as part of this work was carried out on the Dutch national e-infrastructure. This research used the ALICE high-performance computing facility at the University of Leicester for the GOSAT retrievals. We thank the Japanese Aerospace Exploration Agency, National Institute for Environmental Studies and the Ministry of Environment for the GOSAT data and their continuous support as part of the Joint Research Agreement. RJP acknowledges funding from the UK National Centre for Earth Observation (Grants: NE/Y006216/1 and NE/W004895/1), the Natural Environment Research Council [Grant: NE/X019071/1, "UK EO Climate Information Service"] and a UKRI Future Leaders Fellowship (Grant: MR/X033139/1).

**References**

Ahluwalia, I. J. and Patel, U.: Solid Waste Management in India An Assessment of Resource Recovery and Environmental Impact, Indian Council for Research on International Economic Relations, 2018. Available at: https://icrier.org/pdf/Working_Paper_356.pdf (last access: 1 December 2025).

Balasus, N., Jacob, D. J., Lorente, A., Maasakkers, J. D., Parker, R. J., Boesch, H., Chen, Z., Kelp, M. M., Nesser, H., and Varon, D. J.: A blended TROPOMI+GOSAT satellite data product for atmospheric methane using machine learning to correct retrieval biases, Atmospheric Measurement Techniques, 16, 3787–3807, https://doi.org/10.5194/amt-16-3787-2023, 2023.

Belikov, D. A., Patra, P. K., Terao, Y., Naja, M., Ahmed, Md. K., and Saitoh, N.: Assessment of the impact of observations at Nainital (India) and Comilla (Bangladesh) on the CH4 flux inversion, Progress in Earth and Planetary Science, 11, 36, https://doi.org/10.1186/s40645-024-00634-x, 2024.

Bhattarai, N., Dahal, S., Thapa, S., Pradhananga, S., Karky, B. S., Rawat, R. S., Windhorst, K., Watanabe, T., Thapa, R. B., and Avtar, R.: Forest Fire in the Hindu Kush Himalayas: A Major Challenge for Climate Action, J. Forest & Livelihood, 21, 14–31, https://doi.org/10.3126/jfl.v21i1.56576, 2022.

Bloom, A. A., Bowman, K. W., Lee, M., Turner, A. J., Schroeder, R., Worden, J. R., Weidner, R. J., Mcdonald, K. C., and Jacob, D. J.: CMS: Global 0.5-deg Wetland Methane Emissions and Uncertainty (WetCHARTs v1.0), ORNL DAAC, https://doi.org/10.3334/ORNLDAAC/1502, 2017.

Bovensmann, H., Burrows, J. P., Buchwitz, M., Frerick, J., Noël, S., Rozanov, V. V., Chance, K. V., and Goede, A. P. H.: SCIAMACHY: Mission Objectives and Measurement Modes, Journal of the Atmospheric Sciences, 56, 127–150, https://doi.org/10.1175/1520-0469(1999)056<0127:SMOAMM>2.0.CO;2, 1999.

Brasseur G. and Jacob, D.: Modeling of Atmospheric Chemistry: https://www.cambridge.org/core/books/modeling-of-atmospheric-chemistry/88C5AEAD7C28EA3E17FFA6D2CE92DE06, (last access: 18 November 2024).

https://doi.org/10.5194/egusphere-2025-6528
Preprint. Discussion started: 16 February 2026


Butz, A., Guerlet, S., Hasekamp, O., Schepers, D., Galli, A., Aben, I., Frankenberg, C., Hartmann, J.-M., Tran, H., Kuze, A., Keppel-Aleks, G., Toon, G., Wunch, D., Wennberg, P., Deutscher, N., Griffith, D., Macatangay, R., Messerschmidt, J., Notholt, J., and Warneke, T.: Toward accurate CO2 and CH4 observations from GOSAT, Geophysical Research Letters, 38, https://doi.org/10.1029/2011GL047888, 2011.

Calisesi, Y., Soebijanta, V. T., and van Oss, R.: Regridding of remote soundings: Formulation and application to ozone profile comparison, Journal of Geophysical Research: Atmospheres, 110, https://doi.org/10.1029/2005JD006122, 2005.

Chandra, N., Hayashida, S., Saeki, T., and Patra, P. K.: What controls the seasonal cycle of columnar methane observed by GOSAT over different regions in India?, Atmospheric Chemistry and Physics, 17, 12633–12643, https://doi.org/10.5194/acp-17-12633-2017, 2017.

Chen, Z., Jacob, D. J., Nesser, H., Sulprizio, M. P., Lorente, A., Varon, D. J., Lu, X., Shen, L., Qu, Z., Penn, E., and Yu, X.: Methane emissions from China: a high-resolution inversion of TROPOMI satellite observations, Atmospheric Chemistry and Physics, 22, 10809–10826, https://doi.org/10.5194/acp-22-10809-2022, 2022.

Climate and Clean air Coalition: Global methane pledge: https:// www.globalmethanepledge.org/, (last access: 16 July 2025.)

Climate TRACE: Tracking Real-time Atmospheric Carbon Emissions, Climate TRACE Emissions Inventory, 2024 available at: https://climatetrace.org, (last access: 30 July 2025).

Chen, Z., Jacob, D. J., Gautam, R., Omara, M., Stavins, R. N., Stowe, R. C., Nesser, H., Sulprizio, M. P., Lorente, A., Varon, D. J., Lu, X., Shen, L., Qu, Z., Pendergrass, D. C., and Hancock, S.: Satellite quantification of methane emissions and oil–gas methane intensities from individual countries in the Middle East and North Africa: implications for climate action, Atmospheric Chemistry and Physics, 23, 5945–5967, https://doi.org/10.5194/acp-23-5945-2023, 2023.

Central Pollution Control Board (CPCB), Ministry of Forest, Environment and Climate Change, Government of India: Guidelines for Disposal of Legacy Waste (Old Municipal Solid Waste), 2019. Available at : https://cpcb.nic.in/uploads/LegacyWasteBiomining_guidelines_29.04.2019.pdf (last access: 2 December 2025).

Dangeti, M. V., Pathakoti, M., Asuri, K. L., Peethani, S., Shaik, I., Krishnan Sundara, R., Sagar, V. K., Pushpanathan, R., Tiwari, Y. K., and Chauhan, P.: Emissions of methane from coal fields, thermal power plants, and wetlands and their implications for atmospheric methane across the south Asian region, Atmospheric Chemistry and Physics, 24, 12843–12859, https://doi.org/10.5194/acp-24-12843-2024, 2024.

Delwiche, K. B., Harrison, J. A., Maasakkers, J. D., Sulprizio, M. P., Worden, J., Jacob, D. J., and Sunderland, E. M.: Estimating Drivers and Pathways for Hydroelectric Reservoir Methane Emissions Using a New Mechanistic Model, Journal of Geophysical Research: Biogeosciences, 127, e2022JG006908, https://doi.org/10.1029/2022JG006908, 2022.

Dogniaux, M., Maasakkers, J. D., Girard, M., Jervis, D., McKeever, J., Schuit, B. J., Sharma, S., Lopez-Noreña, A., Varon, D. J., and Aben, I.: Global satellite survey reveals uncertainty in landfill methane emissions. *Nature* 647, 397–402, doi:10.1038/s41586-025-09683-8,2025.

Duren, R. M., Thorpe, A. K., Foster, K. T., Rafiq, T., Hopkins, F. M., Yadav, V., Bue, B. D., Thompson, D. R., Conley, S., Colombi, N. K., Frankenberg, C., McCubbin, I. B., Eastwood, M. L., Falk, M., Herner, J. D., Croes, B. E., Green, R. O., and Miller, C. E.: California's methane super-emitters, Nature, 575, 180–184, https://doi.org/10.1038/s41586-019-1720-3, 2019.

Estrada, L. A., Varon, D. J., Sulprizio, M., Nesser, H., Chen, Z., Balasus, N., Hancock, S. E., He, M., East, J. D., Mooring, T. A., Oort Alonso, A., Maasakkers, J. D., Aben, I., Baray, S., Bowman, K. W., Worden, J. R., Cardoso-Saldaña, F. J., Reidy, E.,

https://doi.org/10.5194/egusphere-2025-6528
Preprint. Discussion started: 16 February 2026


and Jacob, D. J.: Integrated Methane Inversion (IMI) 2.0: an improved research and stakeholder tool for monitoring total methane emissions with high resolution worldwide using TROPOMI satellite observations, Geoscientific Model Development, 18, 3311–3330, https://doi.org/10.5194/gmd-18-3311-2025, 2025.

Etiope, G., Ciotoli, G., Schwietzke, S., and Schoell, M.: Gridded maps of geological methane emissions and their isotopic signature, Earth System Science Data, 11, 1–22, https://doi.org/10.5194/essd-11-1-2019, 2019.

Express, The Indian: Reclaiming Deonar landfill, moving a mountain, The Indian Express, 2025. Available at: https://indianexpress.com/article/opinion/editorials/reclaiming-deonar-landfill-moving-a-mountain-10063658/ (last access:1 December, 2025).

Foy, B. de, Schauer, J. J., Lorente, A., and Borsdorff, T.: Investigating high methane emissions from urban areas detected by TROPOMI and their association with untreated wastewater, Environ. Res. Lett., 18, 044004, https://doi.org/10.1088/1748-9326/acc118, 2023.

Fung, I., John, J., Lerner, J., Matthews, E., Prather, M., Steele, L. P., and Fraser, P. J.: Three-dimensional model synthesis of the global methane cycle, Journal of Geophysical Research: Atmospheres, 96, 13033–13065, https://doi.org/10.1029/91JD01247, 1991.

Ganesan, A. L., Rigby, M., Lunt, M. F., Parker, R. J., Boesch, H., Goulding, N., Umezawa, T., Zahn, A., Chatterjee, A., Prinn, R. G., Tiwari, Y. K., Van Der Schoot, M., and Krummel, P. B.: Atmospheric observations show accurate reporting and little growth in India's methane emissions, Nat Commun, 8, 836, https://doi.org/10.1038/s41467-017-00994-7, 2017.

Gao, J., Guan, C., Zhang, B., and Li, K.: Decreasing methane emissions from China's coal mining with rebounded coal production, Environ. Res. Lett., 16, 124037, https://doi.org/10.1088/1748-9326/ac38d8, 2021.

Goswami, R. and Ghosh, S.: Baghjan oil blowout: Report indicates a long road to recovery and ecological restoration, Mongabay-India, 2021. Available at: https://india.mongabay.com/2021/07/baghjan-oil-blowout-report-indicates-a-long-road-to-recovery-and-ecological-restoration/, 2021 (accessed 4 December 2025).

Government of India: India's Updated First Nationally Determined Contribution Under Paris Agreement (2021-2023), available at https://unfccc.int/sites/default/files/NDC/2022-08/India%20Updated%20First%20Nationally%20Determined%20Contrib.pdf, 2022 (accessed 4 December 2025).

Guha, N.: Gas leak in Assam oil rig under control but has affected hundreds, Mongabay-India, 2025. Available at https://india.mongabay.com/2025/07/gas-leak-in-assam-oil-rig-under-control-but-has-affected-hundreds/. (accessed 1 December 2025).

Guha, T., Tiwari, Y. K., Valsala, V., Lin, X., Ramonet, M., Mahajan, A., Datye, A., and Kumar, K. R.: What controls the atmospheric methane seasonal variability over India?, Atmospheric Environment, 175, 83–91, https://doi.org/10.1016/j.atmosenv.2017.11.042, 2018.

Guptha, G. C., Swain, S., Al-Ansari, N., Taloor, A. K., and Dayal, D.: Evaluation of an urban drainage system and its resilience using remote sensing and GIS, Remote Sensing Applications: Society and Environment, 23, 100601, https://doi.org/10.1016/j.rsase.2021.100601, 2021.

Hamdan, A., Panda, S., Jain, M. S., Raj, V., and Mathew, S.: Assessing municipal solid waste in Indian smart cities: A path towards Waste-to-Energy, Heliyon, 11, e42770, https://doi.org/10.1016/j.heliyon.2025.e42770, 2025.

https://doi.org/10.5194/egusphere-2025-6528
Preprint. Discussion started: 16 February 2026


Hansen, P. C.: The L-curve and its use in the numerical treatment of inverse problems, in: *Computational Inverse Problems in Electrocardiology*, edited by: Johnston, P., Advances in Computational Bioengineering, WIT Press, Southampton, UK, 119–142, 2001.

Heald, C. L., Jacob, D. J., Jones, D. B. A., Palmer, P. I., Logan, J. A., Streets, D. G., Sachse, G. W., Gille, J. C., Hoffman, R. N., and Nehrkorn, T.: Comparative inverse analysis of satellite (MOPITT) and aircraft (TRACE-P) observations to estimate Asian sources of carbon monoxide, Journal of Geophysical Research: Atmospheres, 109, https://doi.org/10.1029/2004JD005185, 2004.

Hmiel, B., Petrenko, V. V., Dyonisius, M. N., Buizert, C., Smith, A. M., Place, P. F., Harth, C., Beaudette, R., Hua, Q., Yang, B., Vimont, I., Michel, S. E., Severinghaus, J. P., Etheridge, D., Bromley, T., Schmitt, J., Faïn, X., Weiss, R. F., and Dlugokencky, E.: Preindustrial 14CH4 indicates greater anthropogenic fossil CH4 emissions, Nature, 578, 409–412, https://doi.org/10.1038/s41586-020-1991-8, 2020.

Hu, H., Landgraf, J., Detmers, R., Borsdorff, T., Aan de Brugh, J., Aben, I., Butz, A., and Hasekamp, O.: Toward Global Mapping of Methane With TROPOMI: First Results and Intersatellite Comparison to GOSAT, Geophysical Research Letters, 45, 3682–3689, https://doi.org/10.1002/2018GL077259, 2018.

Huang, Y., Natraj, V., Zeng, Z.-C., Kopparla, P., and Yung, Y. L.: Quantifying the impact of aerosol scattering on the retrieval of methane from airborne remote sensing measurements, Atmospheric Measurement Techniques, 13, 6755–6769, https://doi.org/10.5194/amt-13-6755-2020, 2020.

Janardanan, R., Maksyutov, S., Tsuruta, A., Wang, F., Tiwari, Y. K., Valsala, V., Ito, A., Yoshida, Y., Kaiser, J. W., Janssens-Maenhout, G., Arshinov, M., Sasakawa, M., Tohjima, Y., Worthy, D. E. J., Dlugokencky, E. J., Ramonet, M., Arduini, J., Lavric, J. V., Piacentino, S., Krummel, P. B., Langenfelds, R. L., Mammarella, I., and Matsunaga, T.: Country-Scale Analysis of Methane Emissions with a High-Resolution Inverse Model Using GOSAT and Surface Observations, Remote Sensing, 12, 375, https://doi.org/10.3390/rs12030375, 2020.

Kenneth N. Schuldt, John Mund, Tuula Aalto, James B. Abshire, Ken Aikin, Grant Allen, Marcos Andrade, Arlyn Andrews, Francesco Apadula, Sabrina Arnold, Bianca Baier, Peter Bakwin, Jakub Bartyzel, Gilles Bentz, Peter Bergamaschi, Andreas Beyersdorf, Tobias Biermann, Sebastien C. Biraud, Pierre-Eric Blanc, Harald Boenisch, David Bowling, Gordon Brailsford, Willi A. Brand, Dominik Brunner, Thao P. Bui, Benoit Burban, Lukas Bäni, Francescopiero Calzolari, Cecilia S. Chang, Huilin Chen, Gao Chen, Lukasz Chmura, Shane Clark, Sites Climadat, Aurelie Colomb, Roisin Commane, Lino Condori, Franz Conen, Sébastien Conil, Cédric Couret, Paolo Cristofanelli, Emilio Cuevas, Roger Curcoll, Bruce Daube, Kenneth J. Davis, Martine De Mazière, Stephan De Wekker, Jonathan M. Dean-Day, Julian Della Coletta, Marc Delmotte, Tatiana Di Iorio, Elizabeth DiGangi, Joshua P. DiGangi, Russell Dickerson, Michael Elsasser, Lukas Emmenegger, Shuangxi Fang, Grant Forster, James France, Arnoud Frumau, Marta Fuente-Lastra, Michal Galkowski, Luciana V. Gatti, Torsten Gehrlein, Christoph Gerbig, Francois Gheusi, Emanuel Gloor, Daisuke Goto, Tim Griffis, Samuel Hammer, Thomas F. Hanisco, Chad Hanson, László Haszpra, Juha Hatakka, Martin Heimann, Michal Heliasz, Daniela Heltai, Stephan Henne, Arjan Hensen, Christian Hermans, Ove Hermansen, Eric Hintsa, Antje Hoheisel, Jutta Holst, Laura T. Iraci, Viktor Ivakhov, Daniel A. Jaffe, Armin Jordan, Warren Joubert, Hui-Yun Kang, Anna Karion, Stephan R. Kawa, Victor Kazan, Ralph F. Keeling, Petri Keronen, Jooil Kim, Jörg Klausen, Tobias Kneuer, Mi-Young Ko, Pasi Kolari, Katerina Kominkova, Eric Kort, Elena Kozlova, Paul B. Krummel, Dagmar Kubistin, Susan S. Kulawik, Nicolas Kumps, Casper Labuschagne, David H. Lam, Xin Lan, Ray L. Langenfelds, Andrea Lanza, Olivier Laurent, Tuomas Laurila, Thomas Lauvaux, Jost Lavric, Beverly E. Law, Choong-Hoon Lee, John Lee, Irene Lehner, Kari Lehtinen, Reimo Leppert, Ari Leskinen, Markus Leuenberger, W.H. Leung, Ingeborg Levin, Janne Levula, John Lin, Matthias Lindauer, Anders Lindroth, Zoe M. Loh, Morgan Lopez, Chris R. Lunder, Mikaell O. Löfvenius, Toshinobu Machida, Ivan Mammarella, Giovanni Manca, Alistair Manning, Andrew Manning, Michal V. Marek, Per Marklund, Josette E. Marrero, Melissa Y. Martin, Damien Martin, Giordane A. Martins, Hidekazu Matsueda, Kathryn McKain, Harro Meijer, Frank Meinhardt, Lynne Merchant, Jean-Marc Metzger, N. Mihalopoulos, Natasha L. Miles, Charles E. Miller, John B. Miller, Logan Mitchell, Vanessa Monteiro, Stephen Montzka, Heiko Moossen, Caisa Moreno, Eric

Morgan, Josep-Anton Morgui, Shinji Morimoto, J. W. Munger, David Munro, Mathew Mutuku, Cathrine L. Myhre, Meelis Mölder, Jennifer Müller-Williams, Shin-Ichiro Nakaoka, Jaroslaw Necki, Sally Newman, Sylvia Nichol, Euan Nisbet, Yosuke Niwa, David M. Njiru, Steffen M. Noe, Yukihiro Nojiri, Simon O\'Doherty, Florian Obersteiner, Bill Paplawsky, Caroline L. Parworth, Jeff Peischl, Olli Peltola, Wouter Peters, Carole Philippon, Salvatore Piacentino, Jean M. Pichon, Penelope Pickers, Steve Piper, Joseph Pitt, Christian Plass-Dülmer, Stephen M. Platt, Steve Prinzivalli, Michel Ramonet, Ramon Ramos, Xinrong Ren, Enrique Reyes-Sanchez, Scott J. Richardson, Louis-Jeremy Rigouleau, Haris Riris, Pedro P. Rivas, Michael Rothe, Yves-Alain Roulet, Thomas Ryerson, Ju-Mee Ryoo, Maryann Sargent, Motoki Sasakawa, Hinrich Schaefer, Bert Scheeren, Martina Schmidt, Tanja Schuck, Marcus Schumacher, Jennifer Seibel, Thomas Seifert, Mahesh K. Sha, Paul Shepson, Daegeun Shin, Michael Shook, Christopher D. Sloop, Dan Smale, Paul D. Smith, Gerard Spain, Jason M. St. Clair, David Steger, Martin Steinbacher, Britton Stephens, Colm Sweeney, Lise L. Sørensen, Risto Taipale, Shinya Takatsuji, Pieter Tans, Kirk Thoning, Helder Timas, Margaret Torn, Pamela Trisolino, Jocelyn Turnbull, Alex Vermeulen, Brian Viner, Gabriela Vitkova, Stephen Walker, Andrew Watson, Ray Weiss, Dietmar Weyrauch, Steven C. Wofsy, Justin Worsey, Doug Worthy, Irène Xueref-Remy, Emma L. Yates, Dickon Young, Camille Yver-Kwok, Sönke Zaehle, Andreas Zahn, Christoph Zellweger, Miroslaw Zimnoch, Rodrigo A. de Souza, Alcide G. di Sarra, Danielle van Dinther, Pim van den Bulk: Multi-laboratory compilation of atmospheric carbon dioxide data for the period 1957-2023; obspack_co2_1_GLOBALVIEWplus_v10.1_2024-11-13; NOAA Earth System Research Laboratory, Global Monitoring Laboratory: http://doi.org/10.25925/20241101, last access: 3 June 2025.

Kumar, S., Smith, S. R., Fowler, G., Velis, C., Kumar, S. J., Arya, S., Rena, Kumar, R., and Cheeseman, C.: Challenges and opportunities associated with waste management in India, Royal Society Open Science, 4, 160764, https://doi.org/10.1098/rsos.160764, 2017.

Kuze, A., Suto, H., Nakajima, M., and Hamazaki, T.: Thermal and near infrared sensor for carbon observation Fourier-transform spectrometer on the Greenhouse Gases Observing Satellite for greenhouse gases monitoring, Appl. Opt., AO, 48, 6716–6733, https://doi.org/10.1364/AO.48.006716, 2009.

Lorente, A., Borsdorff, T., Butz, A., Hasekamp, O., aan de Brugh, J., Schneider, A., Wu, L., Hase, F., Kivi, R., Wunch, D., Pollard, D. F., Shiomi, K., Deutscher, N. M., Velazco, V. A., Roehl, C. M., Wennberg, P. O., Warneke, T., and Landgraf, J.: Methane retrieved from TROPOMI: improvement of the data product and validation of the first 2 years of measurements, Atmospheric Measurement Techniques, 14, 665–684, https://doi.org/10.5194/amt-14-665-2021, 2021.

Lorente, A., Borsdorff, T., Martinez-Velarte, M. C., and Landgraf, J.: Accounting for surface reflectance spectral features in TROPOMI methane retrievals, Atmospheric Measurement Techniques, 16, 1597–1608, https://doi.org/10.5194/amt-16-1597-2023, 2023.

Lu, X., Jacob, D. J., Wang, H., Maasakkers, J. D., Zhang, Y., Scarpelli, T. R., Shen, L., Qu, Z., Sulprizio, M. P., Nesser, H., Bloom, A. A., Ma, S., Worden, J. R., Fan, S., Parker, R. J., Boesch, H., Gautam, R., Gordon, D., Moran, M. D., Reuland, F., Villasana, C. A. O., and Andrews, A.: Methane emissions in the United States, Canada, and Mexico: evaluation of national methane emission inventories and 2010–2017 sectoral trends by inverse analysis of in situ (GLOBALVIEWplus $CH_4$ ObsPack) and satellite (GOSAT) atmospheric observations, Atmospheric Chemistry and Physics, 22, 395–418, https://doi.org/10.5194/acp-22-395-2022, 2022.

Ma, S., Worden, J. R., Bloom, A. A., Zhang, Y., Poulter, B., Cusworth, D. H., Yin, Y., Pandey, S., Maasakkers, J. D., Lu, X., Shen, L., Sheng, J., Frankenberg, C., Miller, C. E., and Jacob, D. J.: Satellite Constraints on the Latitudinal Distribution and Temperature Sensitivity of Wetland Methane Emissions, AGU Advances, 2, e2021AV000408, https://doi.org/10.1029/2021AV000408, 2021.

Maasakkers, J. D., Jacob, D. J., Sulprizio, M. P., Scarpelli, T. R., Nesser, H., Sheng, J.-X., Zhang, Y., Hersher, M., Bloom, A. A., Bowman, K. W., Worden, J. R., Janssens-Maenhout, G., and Parker, R. J.: Global distribution of methane emissions, emission trends, and OH concentrations and trends inferred from an inversion of GOSAT satellite data for 2010–2015, Atmospheric Chemistry and Physics, 19, 7859–7881, https://doi.org/10.5194/acp-19-7859-2019, 2019.

https://doi.org/10.5194/egusphere-2025-6528
Preprint. Discussion started: 16 February 2026


Maasakkers, J. D., Varon, D. J., Elfarsdóttir, A., McKeever, J., Jervis, D., Mahapatra, G., Pandey, S., Lorente, A., Borsdorff, T., Foorthuis, L. R., Schuit, B. J., Tol, P., van Kempen, T. A., van Hees, R., and Aben, I.: Using satellites to uncover large methane emissions from landfills, Science Advances, 8, eabn9683, https://doi.org/10.1126/sciadv.abn9683, 2022.Available at: https://unfccc.int/documents/645149 (last access:[January 2025]).

Mathew, T. A., Pillai, D., Sukumaran, J., Deshpande, M. V., Buchwitz, M., Schneising, O., Thilakan, V., Ravi, A., Kanakkassery, S. B., Sijikumar, S., Girach, I. A., and Babu, S. S.: Leveraging TROPOMI observations and WRF-GHG modeling to improve methane emission assessments in India, EGUsphere [preprint], https://doi.org/10.5194/egusphere-2025-1977, 5 June 2025.

Ministry of Environment, Forest and Climate Change (MoEFCC): *Annex AS57*, 2021. Available at: https://sansad.in/getFile/annex/255/AS57.pdf?source=pqars, (last access: December 2025).

Ministry of Environment, Forest and Climate Change (MoEFCC): Draft solid waste management rules 2024, 2024. Available at: https://egazette.gov.in/writeReadData/2024/259407.pdf (last access: December 2025).

Ministry of Housing and Urban Affairs (MoHUA), Government of India: Swachh Bharat Mission - Urban 2.0 Operational Guidelines, 2021. Available at: https://sbmurban.org/storage/app/media/pdf/swachh-bharat-2.pdf (last access: December 2025).

Ministry of Environment, Forest and Climate Change (MoEFCC): India Fourth Biennial Update Report to The United Nations Framework Convention on Climate Change, 2024. Available at: https://unfccc.int/sites/default/files/resource/India%20BUR-4.pdf(last access: December 2025).

Ministry of Environment, Forest and Climate Change (MoEFCC): Initial National Communication to the United Nations Framework Convention on Climate change, NATCOM report, MOEFCC, New Delhi, 2004. Available at: https://unfccc.int/resource/docs/natc/indnc1.pdf (last access: July 2025).

Ministry of Fisheries, Animal Husbandry and Dairying, Government of India: 20th Livestock Census – All India Report, Department of Animal Husbandry and Dairying, New Delhi, India, 2019. Available at: https://dahd.nic.in/en/document/20th-livestock-census-2019 (last access: June,2025).

Mohanty, S. and Dutta, R.: India's ONGC says new projects to reverse declining oil output from matured fields, S&P Global Commodity Insights, 2023. Available at: https://www.spglobal.com/commodity-insights/en/news-research/latest-news/crude-oil/111423-indias-ongc-says-new-projects-to-reverse-declining-oil-output-from-matured-fields (last access: 1 December 2025).

Nathan, B., Maasakkers, J. D., Naus, S., Gautam, R., Omara, M., Varon, D. J., Sulprizio, M. P., Estrada, L. A., Lorente, A., Borsdorff, T., Parker, R. J., and Aben, I.: Assessing methane emissions from collapsing Venezuelan oil production using TROPOMI, Atmospheric Chemistry and Physics, 24, 6845–6863, https://doi.org/10.5194/acp-24-6845-2024, 2024.

Nesser, H., Jacob, D. J., Maasakkers, J. D., Scarpelli, T. R., Sulprizio, M. P., Zhang, Y., and Rycroft, C. H.: Reduced-cost construction of Jacobian matrices for high-resolution inversions of satellite observations of atmospheric composition, Atmospheric Measurement Techniques, 14, 5521–5534, https://doi.org/10.5194/amt-14-5521-2021, 2021.

NITI Aayog: Urban Wastewater Scenario in India, White Paper, NITI Aayog, New Delhi, India, 2022.Available at: https://www.niti.gov.in/sites/default/files/2022-09/Waste-Water-A4_20092022.pdf (last access: 23 December 2025).

https://doi.org/10.5194/egusphere-2025-6528
Preprint. Discussion started: 16 February 2026


Nomura, S., Naja, M., Ahmed, M. K., Mukai, H., Terao, Y., Machida, T., Sasakawa, M., and Patra, P. K.: Measurement report: Regional characteristics of seasonal and long-term variations in greenhouse gases at Nainital, India, and Comilla, Bangladesh, Atmospheric Chemistry and Physics, 21, 16427–16452, https://doi.org/10.5194/acp-21-16427-2021, 2021.

Parker, R. J., Webb, A., Boesch, H., Somkuti, P., Barrio Guillo, R., Di Noia, A., Kalaitzi, N., Anand, J. S., Bergamaschi, P., Chevallier, F., Palmer, P. I., Feng, L., Deutscher, N. M., Feist, D. G., Griffith, D. W. T., Hase, F., Kivi, R., Morino, I., Notholt, J., Oh, Y.-S., Ohyama, H., Petri, C., Pollard, D. F., Roehl, C., Sha, M. K., Shiomi, K., Strong, K., Sussmann, R., Té, Y., Velazco, V. A., Warneke, T., Wennberg, P. O., and Wunch, D.: A decade of GOSAT Proxy satellite $CH_4$ observations, Earth System Science Data, 12, 3383–3412, https://doi.org/10.5194/essd-12-3383-2020, 2020.

Panda, M., Equeenuddin, Sk. Md., and Mohanty, D.: Organic petrography and stable isotopic characteristics of Permian Talcher coal, India: Implications on depositional environment, International Journal of Coal Geology, 264, 104130, https://doi.org/10.1016/j.coal.2022.104130, 2022.

Priya, S. and Gupta, S.: The State of Informal Waste Workers in India, SPRF India, 2019.Available at: https://sprf.in/wp-content/uploads/2021/02/19.8.2020_The-State-of-Informal-Waste-Workers-In-India.pdf (last access : 1 December, 2025).

Rajan, K., Khudsar, F. A., and Kumar, R.: Spatio-temporal patterns of microplastic contamination in surface waters of Hooghly River Estuary: Causes and consequences, Regional Studies in Marine Science, 65, 103111, https://doi.org/10.1016/j.rsma.2023.103111, 2023.

Raju, A., Sijikumar, S., Valsala, V., Tiwari, Y. K., Halder, S., Girach, I. A., Jain, C. D., and Ratnam, M. V.: Regional estimation of methane emissions over the peninsular India using atmospheric inverse modelling, Environ Monit Assess, 194, 647, https://doi.org/10.1007/s10661-022-10323-1, 2022.

Ravish, P.: Sustainable Management of Landfill Sites in India: Addressing Environmental, Health, and Socioeconomic Challenges, Current World Environment, 20, 19–34, https://doi.org/10.12944/CWE.20.1.3, 2025.

Rodgers, C. D.: Inverse Methods for Atmospheric Sounding | Series on Atmospheric, Oceanic and Planetary Physics: https://www.worldscientific.com/doi/epdf/10.1142/3171, (last access: 18 November 2024).

Sadavarte, P., Pandey, S., Maasakkers, J. D., Lorente, A., Borsdorff, T., Denier van der Gon, H., Houweling, S., and Aben, I.: Methane Emissions from Superemitting Coal Mines in Australia Quantified Using TROPOMI Satellite Observations, Environ. Sci. Technol., 55, 16573–16580, https://doi.org/10.1021/acs.est.1c03976, 2021.

Sahu, R. K., Hari, M., and Tyagi, B.: Forest Fire Induced Air Pollution over Eastern India during March 2021, Aerosol Air Qual. Res., 22, 220084, https://doi.org/10.4209/aaqr.220084, 2022.

Samal, A., Sahu, S. K., Mishra, A., Mangaraj, P., Pan, S. K., and Beig, G.: Assessment and Quantification of Methane Emission from Indian Livestock and Manure Management, Aerosol Air Qual. Res., 24, 230204, https://doi.org/10.4209/aaqr.230204, 2024.

Saunois, M., Martinez, A., Poulter, B., Zhang, Z., Raymond, P. A., Regnier, P., Canadell, J. G., Jackson, R. B., Patra, P. K., Bousquet, P., Ciais, P., Dlugokencky, E. J., Lan, X., Allen, G. H., Bastviken, D., Beerling, D. J., Belikov, D. A., Blake, D. R., Castaldi, S., Crippa, M., Deemer, B. R., Dennison, F., Etiope, G., Gedney, N., Höglund-Isaksson, L., Holgerson, M. A., Hopcroft, P. O., Hugelius, G., Ito, A., Jain, A. K., Janardanan, R., Johnson, M. S., Kleinen, T., Krummel, P. B., Lauerwald, R., Li, T., Liu, X., McDonald, K. C., Melton, J. R., Mühle, J., Müller, J., Murguia-Flores, F., Niwa, Y., Noce, S., Pan, S., Parker, R. J., Peng, C., Ramonet, M., Riley, W. J., Rocher-Ros, G., Rosentreter, J. A., Sasakawa, M., Segers, A., Smith, S. J., Stanley, E. H., Thanwerdas, J., Tian, H., Tsuruta, A., Tubiello, F. N., Weber, T. S., van der Werf, G. R., Worthy, D. E. J., Xi,

https://doi.org/10.5194/egusphere-2025-6528
Preprint. Discussion started: 16 February 2026


Y., Yoshida, Y., Zhang, W., Zheng, B., Zhu, Q., Zhu, Q., and Zhuang, Q.: Global Methane Budget 2000–2020, Earth Syst. Sci. Data, 17, 1873–1958, https://doi.org/10.5194/essd-17-1873-2025, 2025.

Scarpelli, T. R., Jacob, D. J., Maasakkers, J. D., Sulprizio, M. P., Sheng, J.-X., Rose, K., Romeo, L., Worden, J. R., and Janssens-Maenhout, G.: A global gridded (0.1° × 0.1°) inventory of methane emissions from oil, gas, and coal exploitation based on national reports to the United Nations Framework Convention on Climate Change, Earth System Science Data, 12, 563–575, https://doi.org/10.5194/essd-12-563-2020, 2020.

Schneising, O., Buchwitz, M., Hachmeister, J., Vanselow, S., Reuter, M., Buschmann, M., Bovensmann, H., and Burrows, J. P.: Advances in retrieving XCH 4 and XCO from Sentinel-5 Precursor: improvements in the scientific TROPOMI/WFMD algorithm, Atmospheric Measurement Techniques, 16, 669–694, https://doi.org/https://doi.org/10.5194/amt-16-669-2023, 2023.

Schuit, B. J., Maasakkers, J. D., Bijl, P., Mahapatra, G., van den Berg, A.-W., Pandey, S., Lorente, A., Borsdorff, T., Houweling, S., Varon, D. J., McKeever, J., Jervis, D., Girard, M., Irakulis-Loitxate, I., Gorroño, J., Guanter, L., Cusworth, D. H., and Aben, I.: Automated detection and monitoring of methane super-emitters using satellite data, Atmospheric Chemistry and Physics, 23, 9071–9098, https://doi.org/10.5194/acp-23-9071-2023, 2023.

Shahid, M., Mohanty, S., Munda, S., Chatterjee, D., Khanam, R., Priyadarsini, S., Tripathi, R., and Nayak, A. K.: Sustainable Rice-Based Cropping Systems: Strategies to Minimize Environmental Impact, National Rice Research Institute, 2024.Available at: https://icar-nrri.in/wp-content/uploads/2024/08/NRRI_Research-Bulletin-No-56.pdf (last access: [July 2025]).

Shen, L., Zavala-Araiza, D., Gautam, R., Omara, M., Scarpelli, T., Sheng, J., Sulprizio, M. P., Zhuang, J., Zhang, Y., Qu, Z., Lu, X., Hamburg, S. P., and Jacob, D. J.: Unravelling a large methane emission discrepancy in Mexico using satellite observations, Remote Sensing of Environment, 260, 112461, https://doi.org/10.1016/j.rse.2021.112461, 2021.

Shen, L., Jacob, D. J., Gautam, R., Omara, M., Scarpelli, T. R., Lorente, A., Zavala-Araiza, D., Lu, X., Chen, Z., and Lin, J.: National quantifications of methane emissions from fuel exploitation using high resolution inversions of satellite observations, Nat Commun, 14, 4948, https://doi.org/10.1038/s41467-023-40671-6, 2023.

Siddiqui, A., Halder, S., Kannemadugu, H. B. S., Prakriti, and Chauhan, P.: Detecting Methane Emissions from Space Over India: Analysis Using EMIT and Sentinel-5P TROPOMI Datasets, J Indian Soc Remote Sens, 52, 1901–1921, https://doi.org/10.1007/s12524-024-01925-y, 2024.

Simpson, M., Oduro-Appiah, K., Gunsilius, E., Dias, S. M., and Scheinberg, A.: Shifting perceptions of informal operators in the service and value chains: A retrospective of 40 years of observation and advocacy for informal recyclers and waste service providers, through the eyes of five global participant-researchers, Waste Management & Research, 43, 850–896, https://doi.org/10.1177/0734242X241280076, 2025.

Singh, R.: Methane emissions from Indian landfills: Knowing why estimates vary by models key to effective management, Down To Earth, 2023 Available at: https://www.downtoearth.org.in/waste/methane-emissions-from-indian-landfills-knowing-why-estimates-vary-by-models-key-to-effective-management-91991 (last access: November 2025).

Singhal, A., Gupta, A. K., Dubey, B., and Ghangrekar, M. M.: Seasonal characterization of municipal solid waste for selecting feasible waste-treatment technology for Guwahati city, India, Journal of the Air & Waste Management Association, 72, 147–160, https://doi.org/10.1080/10962247.2021.1980450, 2022.

https://doi.org/10.5194/egusphere-2025-6528
Preprint. Discussion started: 16 February 2026


Skeie, R. B., Hodnebrog, Ø., and Myhre, G.: Trends in atmospheric methane concentrations since 1990 were driven and modified by anthropogenic emissions, Commun Earth Environ, 4, 1–14, https://doi.org/10.1038/s43247-023-00969-1, 2023.

Solanki, S., Chakraborty, M., Dutt, R., Menon, R., Gupta, S., and Mehta, R.: Greenhouse Gas Emission Estimates from AFOLU (Agriculture, Forestry and Other Land Use) Sector in India at the Subnational Level (Version/edition 4.0). New Delhi. GHG Platform India Report – Vasudha Foundation. (4.0), 2022.Available at: https://www.ghgplatform-india.org/afolu-sector/. (last access: November 2024).

Somkuti, P., McGarragh, G. M., O'Dell, C., Di Noia, A., Vogel, L., Crowell, S., Ott, L. E., and Bösch, H.: Surface reflectance biases in $XCH_4$ retrievals from the 2.3 μm band are enhanced in the presence of aerosols, Atmospheric Measurement Techniques Discussions, 1–20, https://doi.org/10.5194/amt-2024-145, 2025.

Stavert, A. R., Saunois, M., Canadell, J. G., Poulter, B., Jackson, R. B., Regnier, P., Lauerwald, R., Raymond, P. A., Allen, G. H., Patra, P. K., Bergamaschi, P., Bousquet, P., Chandra, N., Ciais, P., Gustafson, A., Ishizawa, M., Ito, A., Kleinen, T., Maksyutov, S., McNorton, J., Melton, J. R., Müller, J., Niwa, Y., Peng, S., Riley, W. J., Segers, A., Tian, H., Tsuruta, A., Yin, Y., Zhang, Z., Zheng, B., and Zhuang, Q.: Regional trends and drivers of the global methane budget, Global Change Biology, 28, 182–200, https://doi.org/10.1111/gcb.15901, 2022.

Subramanian, R., Thompson, R. L., Vojta, M., Schneising, O., and Stohl, A.: Strong monsoon influence on South Asian methane emissions in 2020 revealed by a Bayesian inversion constrained by satellite observations, EGUsphere [preprint], https://doi.org/10.5194/egusphere-2025-5108, 14 November 2025.

Forster, P. M., Storelvmo, T., Armour, K., Collins, W., Dufresne, J.-L., Frame, D., Lunt, D. J., Mauritsen, T., Palmer, M. D., Watanabe, M., Wild, M., and Zhang, H.:The Earth's Energy Budget, Climate Feedbacks and Climate Sensitivity (Chapter 7) - Climate Change 2021 – The Physical Science Basis: https://www.cambridge.org/core/books/climate-change-2021-the-physical-science-basis/earths-energy-budget-climate-feedbacks-and-climate-sensitivity/AE57C97E588FF3060C7C7E47DD4F3C6E, (last access: 6 December 2024).

Thorpe, A. K., Green, R. O., Thompson, D. R., Brodrick, P. G., Chapman, J. W., Elder, C. D., Irakulis-Loitxate, I., Cusworth, D. H., Ayasse, A. K., Duren, R. M., Frankenberg, C., Guanter, L., Worden, J. R., Dennison, P. E., Roberts, D. A., Chadwick, K. D., Eastwood, M. L., Fahlen, J. E., and Miller, C. E.: Attribution of individual methane and carbon dioxide emission sources using EMIT observations from space, Science Advances, 9, eadh2391, https://doi.org/10.1126/sciadv.adh2391, 2023.

Lan, X., K.W. Thoning, and E.J. Dlugokencky: Trends in globally averaged CH4, N2O, and SF6 determined from NOAA Global Monitoring Laboratory measurements. Version 2025-11: https://gml.noaa.gov/ccgg/trends_ch4/index.html, last access: 16 July 2025.

Varon, D. J., Jacob, D. J., Sulprizio, M., Estrada, L. A., Downs, W. B., Shen, L., Hancock, S. E., Nesser, H., Qu, Z., Penn, E., Chen, Z., Lu, X., Lorente, A., Tewari, A., and Randles, C. A.: Integrated Methane Inversion (IMI 1.0): a user-friendly, cloud-based facility for inferring high-resolution methane emissions from TROPOMI satellite observations, Geoscientific Model Development, 15, 5787–5805, https://doi.org/10.5194/gmd-15-5787-2022, 2022.

van der Werf, G. R., Randerson, J. T., Giglio, L., van Leeuwen, T. T., Chen, Y., Rogers, B. M., Mu, M., van Marle, M. J. E., Morton, D. C., Collatz, G. J., Yokelson, R. J., and Kasibhatla, P. S.: Global fire emissions estimates during 1997–2016, Earth System Science Data, 9, 697–720, https://doi.org/10.5194/essd-9-697-2017, 2017.

Wright, C., Patel, B., Modadugu, R., Setawan, D., and Yeman, C.: Coal mine methane's critical moment in India, Ember, 2024. Available at: https://ember-energy.org/latest-insights/coal-mine-methanes-critical-moment-in-india,(last access: December 2025).

https://doi.org/10.5194/egusphere-2025-6528
Preprint. Discussion started: 16 February 2026


World Population Dashboard -India | United Nations Population Fund: https://www.unfpa.org/data/world-population/IN, last access: 22 January 2026.

Yuan, B., Kaser, L., Karl, T., Graus, M., Peischl, J., Campos, T. L., Shertz, S., Apel, E. C., Hornbrook, R. S., Hills, A., Gilman, J. B., Lerner, B. M., Warneke, C., Flocke, F. M., Ryerson, T. B., Guenther, A. B., and de Gouw, J. A.: Airborne flux measurements of methane and volatile organic compounds over the Haynesville and Marcellus shale gas production regions, Journal of Geophysical Research: Atmospheres, 120, 6271–6289, https://doi.org/10.1002/2015JD023242, 2015.

Zhang, X., Maasakkers, J. D., Roger, J., Guanter, L., Sharma, S., Lama, S., Tol, P., Varon, D. J., Cusworth, D. H., Howell, K., Thorpe, A. K., Brodrick, P. G., and Aben, I.: Global Identification of Solid Waste Methane Super Emitters Using Hyperspectral Satellites, Environ. Sci. Technol., acs.est.4c14196, https://doi.org/10.1021/acs.est.4c14196, 2025.

Zhang, Y., Jacob, D. J., Lu, X., Maasakkers, J. D., Scarpelli, T. R., Sheng, J.-X., Shen, L., Qu, Z., Sulprizio, M. P., Chang, J., Bloom, A. A., Ma, S., Worden, J., Parker, R. J., and Boesch, H.: Attribution of the accelerating increase in atmospheric methane during 2010–2018 by inverse analysis of GOSAT observations, Atmospheric Chemistry and Physics, 21, 3643–3666, https://doi.org/10.5194/acp-21-3643-2021, 2021.

Zhu, D., Asnani, P. U., Zurbrugg, C., Anapolsky, S., and Mani, S.: Improving Municipal Solid Waste Management in India: A Sourcebook for Policy Makers and Practitioners, World Bank, Washington, DC, 2012. Available at: https://documents1.worldbank.org/curated/en/682051468267572634/pdf/425660PUB0Wast12732601OFFICIAL0USE1.pdf (last access: 1 December, 2025).